HIGH GRADIENT MAGNETIC SEPARATION OF NANOSCALE MAGNETITE

by

PAUL C. OWINGS

B.S., Kansas State University, 2009

A THESIS

submitted in partial fulfillment of the requirements for the degree

MASTER OF SCIENCE

Department of Civil Engineering
College of Science

KANSAS STATE UNIVERSITY
Manhattan, Kansas

2011

Approved by:

Major Professor
Dr. Alexander Mathews

Copyright

Abstract

Nanoscale magnetite is being examined for possible uses as an adsorbent of heavy metals and for the enhancement of water treatment processes such as stripping of trichloroethylene (TCE) from contaminated water supplies and wastewaters. Methods for recovering nanoscale magnetite must be developed before the particles can be used in water treatment processes. This is necessary because expelling high amounts of particles into the environment will be unacceptable and costly; if captured they can be reused; additionally, they could potentially cause environmental impacts due to their stability in an aqueous environment and possible toxicity. Nanoscale magnetite is superparamagnetic, so it has a high magnetic susceptibility, and hence it is very attracted to magnetized materials. Utilizing the magnetic properties of magnetite may be one possible means of separating the particles from a treatment process. High Gradient Magnetic Separation (HGMS) has been studied for the separation of micron and even tenths of a micron size particles, but there is little experimental data for HGMS of nanoscale magnetite. This research looks to filter nanoscale magnetite through a HGMS and determine the capture efficiency of the filter. Subsequently, the filter was backwashed to determine particle recover efficiencies. The flow rate was adjusted to determine the dependency of particle capture efficiency on cross sectional velocity through the filter. Additionally, particle loading was changed to better understand the correlation of particle loading with capture efficiency. Filtrations for nanoscale magnetite dispersed with sodium tripolyphosphate were also completed as well as filtrations of nanoscale magnetite coated with silica and magnetite silica composites.

Experimental data in this research indicates that magnetite nanoparticles can be captured at 99.8% efficiency or higher in a well-designed filtration system. Capture efficiencies around 99.8% have been found for magnetite. The silica coated magnetite and magnetite silica composites were captured at efficiencies as high as 96.7% and 97.9%, respectively. The capture efficiency of the dispersed magnetite is lower than non-dispersed magnetite and most promising at relatively low fluid flow velocities and particle loadings. The maximum capture efficiency for dispersed magnetite particles was 90.3%. Both magnetite and dispersed magnetite were successfully recovered using backwash at pH of 10 to 11.

Table of Contents

List of Figures

List of Tables

Acknowledgements

My major professor Dr. Alexander Mathews, played an essential in the development and completion of all aspects of this project. Dr. Kenneth Klabunde and Dr. Damber Hamal from the chemistry department played an important role in the analysis of data and provided me with all silica/magnetite samples. Dr. Jennifer Anthony from the department of chemical engineering, allowed me to use her atomic absorber to analyze samples. James Ewing and Shashi Kambhampati assisted me in the lab and played a role in the development of the gravity fed filter. Ryan Bentman constructed apparatuses used in the lab.

Dedication

I would like to dedicate this thesis to my mother and father who have supported me throughout its completion.

Chapter 1
Introduction

Problem discussion

Nanoscale magnetite particles have useful properties that make them a prime candidate for industrial applications. If nanoscale magnetite is to be incorporated into industrial processes it is necessary to be able to capture and reuse the particles. Nanoscale magnetite exhibits superparamagnetic properties so they interact rather strongly with magnets. Thus using magnetic separation methods is feasible for their capture. High Gradient Magnetic Separation (HGMS) is one magnetic separation method which employs high localized magnetic gradients throughout the cross section of a column by magnetizing a media, typically stainless steel wool, within the column.

The dominating principle behind HGMS is the magnetic force must overcome other forces for a particle to be successfully captured. The force exerted on a particle from a magnetized wire can be represented as follows where μ_o is the permeability of free space, M_p is the magnetization of the particles, V_p is the volume of the particle, and ∇H is the magnetic field gradient induced by the magnetized wire at the position of the particle (Moeser, 2004; Ditsch, 2005).

$$\mathbf{F_m=\mu_o M_p V_p \times \nabla\ (H)} \qquad (1)$$

Since the magnetic force is proportional to the volume of the particle, smaller particles are increasingly difficult to capture. Others have performed bench scale HGMS of nanoscale magnetite composites (Moeser 2004), magnetite clusters (Ditsch, 2005), and magnetite particles (Yavuz[1] 2006; Yavuz[2] 2006). This research will supplement previously completed bench scale HGMS of nanoscale magnetite by completing magnetic filtrations with a different experimental setup. Supplementing the completed research under different conditions will expand upon the base of knowledge and allow for a better assessment of the feasibility of the HGMS of nanoscale magnetite. Additionally, by researching the effects of different parameters on the capture efficiency of nanoscale magnetite particles, the limitations of the technology can be determined.

In this research, magnetite water slurries were created by sonicating the mixture. The particle size in the supernatant was determined by Dambar Hamal to be 15-20 nm by direct light scattering. The slurries were pumped through a Frantz Ferrofilter Model PRE-1. The particle concentration in the effluent was determined by dissolving the particles with concentrated hydrochloric or nitric acid and analyzing the sample for total iron using spectrophotometry or atomic adsorption. After obtaining the total iron concentration, the amount of magnetite was determining using stoichiometry from the dissolution reaction.

Several parameters were varied to determine their correlation with the performance of the filter. The different parameters that were evaluated were flowrate or velocity through the cross section of the column, the particle loading or concentration of particles in solution, and the effect of magnetite particles coated with silica and magnetite particles dispersed with sodium tripolyphosphate. Filtering the particles in series was also performed to determine the effect of multiple passes through the filter. Determining the effect of velocity on the capture efficiency provides valuable insight on the rate limitations of the process and required residence time for capture. In industrial applications, the particle loading passing through the filter will most likely vary. Therefore examining the effect of particle loading on capture efficiency is important. Nanoscale magnetite is often functionalized to stabilize the particles (Wooding, 1991; Shen, 1999) or provide desirable surface conditions (Moeser, 2002). As functionalizing the particles is common it is important to determine the effects that functionalization has on particle capture. So magnetite particles coated with silica were filtered. Another means of stabilizing particles is by adding a dispersant, and like functionalized particles, if a dispersant is to be used, information on the effect of the dispersant on the recoverability of the particle is needed. Completing a filtration in series gave insight into whether the capture efficiency was solely limited by particle size or if residence time had some effect on the capture efficiency. In addition to filtrations, backwashes were completed to determine the conditions required for successful backwash. For backwashes, the flowrate was varied to determine the required flowrate for recovery.

Alternative removal methods

Different methods for the capture of nanoscale magnetite have been explored. Some of the alternative methods for the removal of nanoscale magnetite are sedimentation based removal (Chin, 2006; Stolarski, 2007; Zhang, 2008) and expanded bed adsorption (EBA) (Hubbuch,

2001). These methods can be observed and compared with HGMS to determine which is most suitable for a given process.

Sedimentation based process can be classified either as gravity sedimentation for coarse particles or centrifuge for fine particles (Stolarski 2007). As particles become smaller their residence time in solutioni increases and becomes too large for their separation by sedimentation. The settling velocity can be increased by destabilizing the particles so they are attracted to each other and form aggregates; the aggregates are larger and will settle more quickly. One way to destabilize particles is by adjusting the pH to create favorable surface potential for the particles. Another is by magnetizing them so that they are attracted to one another. Either way, the desired effect is for aggregates to form that can be settled or centrifuged out of solution (Stolarski 2007). Stolarski's results show that an increase in particle loading increases the settling velocity as well as magnetization. This can be seen in the figure below for centrifuge separation at various particle loadings (Stolarski 2007).

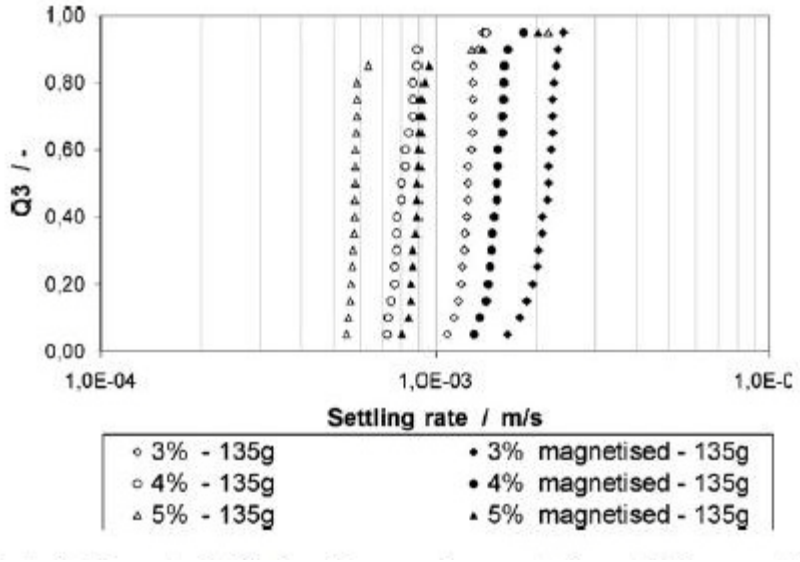

Figure 1. Settling velocity distribution for various particle loadings and magnetized particles, (Stolarski 2007).

As can be seen in the previous figure, magnetized particles have relatively higher settling velocities. Additionally, the maximum settling velocity is approximately 0.2 cm/s. As previously stated, slurries with higher particle concentrations have higher settling velocities due to an increase in particle interaction, which is verified in Figure 2. It does not discuss the feasibility of utilizing centrifuging to remove the particles. One problem with this method is as

particles become smaller, they will not retain any magnetism because as the particle size decreases, superparamagnetic properties (Worm, 1997) are observed. So the particles will have no coercivity and therefore aggregation will be based purely on surface potential.

Another research paper destabilizes a slurry of nanoscale silica by adding magnetite (Chin, 2006). The particles aggregate together because of a high electrostatic attraction between silica and magnetite. Chin's study added magnetite to a silica slurry and observed a change in the turbidity of the supernatant after 1 hour while varying the pH, adding salt, and changing the magnetite particle conditions. The results can be seen in the table below (Chin, 2006).

Table 1. Change in the turbidity of a nanoscale silica magnetite solution, (Chin, 2006).

(a) Time (min)	Solution pH					
	2.0	3.0	4.0	5.0	6.0	7.0
0	18000	15600	15900	15000	14400	16800
60	256	2.4	3.7	7.6	6.9	231
(b) Time (min)	NaCl (M)					
	0	0.004	0.04	0.4		
0	14400	15000	16500	18000		
60	6.9	7.6	9.8	10.2		
(c) Time (min)	Types of magnetite particles					
	Fe_3O_4 slurry	Dried Fe_3O_4	4.5 μm Fe_3O_4			
0	9500	17000	6700			
60	5.9	46.3	89.2			

No addition of magnetic field during sedimentation, original turbidity of the CMP wastewater = 110 NTU, and 10 g of magnetite particles. (a) Influences of solution pH: no addition of salt; (b) Influences of addition of salt: pH = 6; (c) Influences of types of seeding particles: pH = 6 and no addition of salt.

The results show that a pH of 3 gives the optimum reduction in the turbidity of the solution (Chin 2006). Additionally, the presence of salt hampers settling (Chin, 2006). This study shows that the turbidity of the solution can significantly be decreased by consecutive aggregation of nanoscale magnetite and silica. The residence time for the removal is relatively high at 1 hour, and information is not given on the rate at which the particles settle.

Nanoparticles can also be destabilized chemically (Zhang, 2008). Chemicals are added to lower the zeta potential of the particles or destabilize the particles; the suspension is then flocculated to encourage aggregation which can result in faster settling (Zhang, 2008). The particles will form aggregates without the addition of chemicals due to surface interactions (Zhang, 2008). The first method used to destabilize the particles was by adding a high electrolyte concentration of 0.1 M $MgCl_2$,which changed the absolute value of all the zeta potentials to below 10 mV (Zhang, 2008). Four different flocullation times were also used to

determine the effects of flocculation time with a 1 hour sedimentation time (Zhang, 2008). The next approach used was an alum dosage, which is a traditional coagulant in water treatment processes. Doses of 20-60 mg/L were added to the solutions and the particles were settled after coagulation and flocculation (Zhang, 2008). Both chemical treatment methods used 10 mg/L nanoparticles mixtures (Zhang, 2008). The results from these studies show at maximum about 80% removal of particles after a substantial time interval. The following two figures represent the results of coagulation, flocculation, and sedimentations (Zhang, 2008).

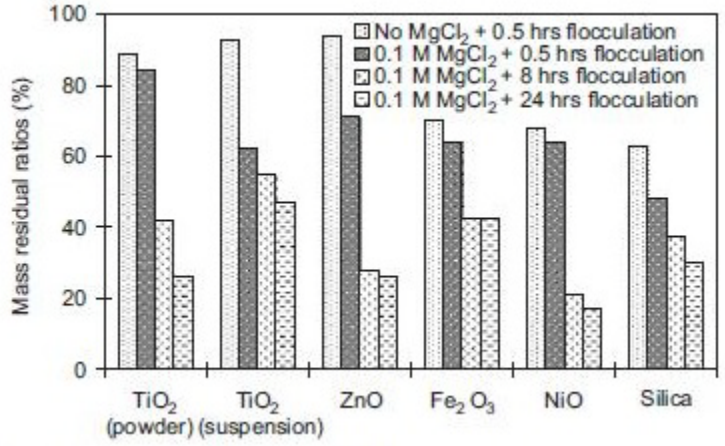

Figure 2. Sedimentation data for 10 mg/L nanoparticles after 1 hour settling, (Zhang, 2008).

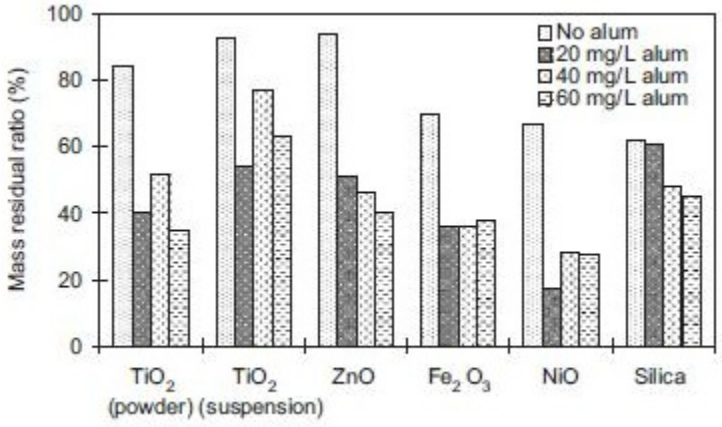

Figure 3. Sedimentation of 10 mg/L nanoparticles with an alum dosage, (Zhang, 2008)

Expanded bed absorption (EBA) typically consist of porous supports with a specific particle size distribution controlled by the density of the media (Hubbuch, 2001). Hubbuch performed a study on EBA to determine if they were more productive than HGMS. The productivity was calculated based on the superficial flow velocity, initial product concentration,

dynamic product capacity, number of adsorptive stages, and the initial magnetic support concentration (Hubbuch, 2001). By comparing the productivity, it was determined that the productivity of HGMS was many times higher than that of EBA (Hubbuch, 2001).

Importance of the Problem

One application of nanoscale magnetite currently being researched is the adsorption of heavy metal ions and (Yavuz[1], 2006; Yantasee, 2007; Liu, 2008; Yuan, 2010) and enhanced stripping of volatile organic compounds. If the particles are to be utilized in a water treatment process, a method for removing the particles from the feed is necessary to prevent the release of particles into the environment, and allow the particles to be recycled. Since removing the particles from the water trains is a major consideration in the implication of nanoscale magnetite into water treatment processes, determining its feasibility is critical. This research looks to develop on the plausibility of the removal and recovery of nanoscale magnetite using HGMS.

Nanoscale magnetite in water treatment

One of the primary reasons that magnetite nanoparticles are of special interest in industrial applications is because they can be controlled by magnetic fields. Additionally, nanoscale magnetite can be produced by a simple precipitation reaction (Martinez-Mera, 2007). Other than having strong magnetic properties, one of the main reasons that nanoscale magnetite is being examined for its use in industrial applications is that it has a high specific surface area. High surface areas are typically conducive of higher reactivity so they can be expected to increase the rate of various processes. As well, materials with high surface areas often have superior adsorbent properties than those with low surface areas as is the case for heavy metals (Jing-Fu, 2008; Yavuz, 2006; Wassana, 2007; Yaun, 2010). The specific area of magnetite compared to particle diameter is shown below (Tratnyek, 2006).

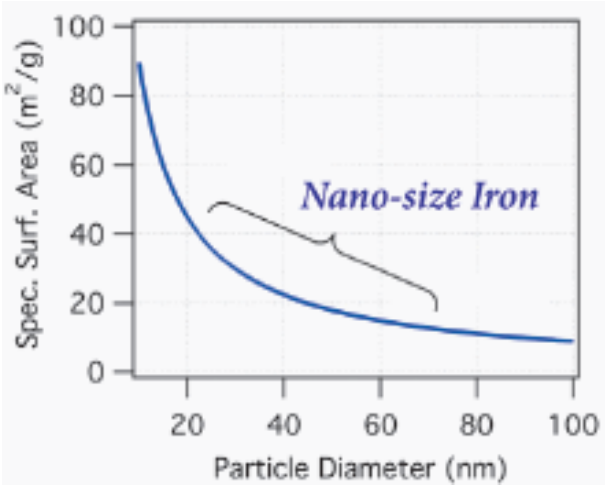

Figure 4. Specific surface area of nanoscale magnetite, (Tratnyek, 2006)

Heavy metals are toxic and exist as a form of water pollution globally (Nriagu, 1988). One of the studied uses of nanoscale magnetite and magnetite composites is an adsorbent of heavy metals (Yavuz[1], 2006; Yantasee, 2007; Liu, 2008; Yuan, 2010). One study (Yavuz[1], 2006) determined the adsorptive capacity of magnetite with size ranging from 300 nm to 12 nm and found that the decrease in size increased the adsorptive capacity by up to 1000 times. Another study (Yantasee, 2007) found that magnetite particles functionalized with dimercaptosuccinic acid (DMSA) and size of about 6 nm had an adsorptive capacity of 227 mg of Hg/g, which was 30 times higher than that of a commercial resin used for adsorption. Additionally, the DMSA-magnetite particles removed 99% of 1 mg/L lead in a minute, while it took 10 to 120 minutes for two other resins to remove 1 mg/L of pollutant (Yantasee, 2007). Liu (2008) reported high removal efficiencies for magnetite coated with Humic acid, 99% for mercury and lead and 95% for copper and cadmium for both natural and tap water at the optimum pH value.

It can be deduced from the previous research that nanoscale magnetite and magnetite composites can be utilized as highly effective adsorbents, both because of increased adsorption rates and adsorptive capacities. If the particles are to be incorporated into water treatment processes, a means of separating the particles from solution needs to be developed, as is completed in this research using HGMS. A schematic of how HGMS would be used in a water treatment process is shown below.

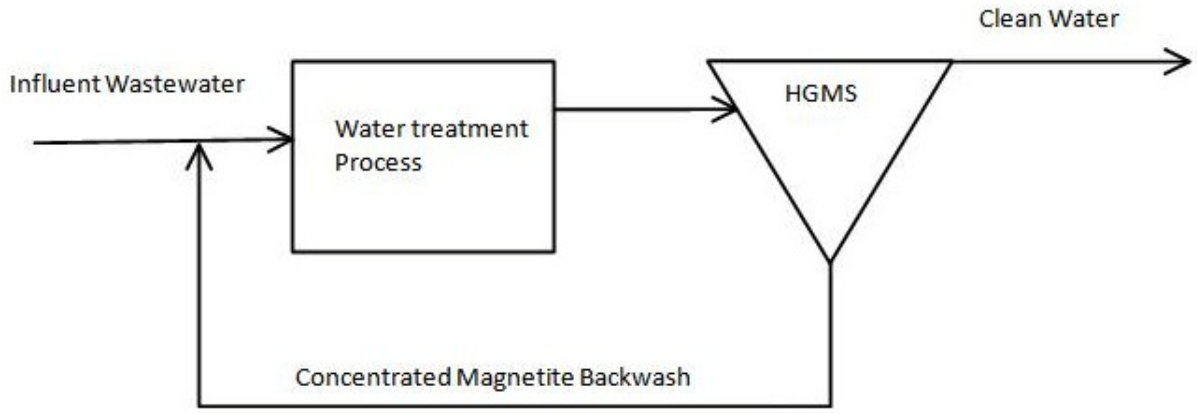

Figure 5. Water treatment process schematic.

A concentrated slurry of the magnetite particles would be added to the influent wastewater stream. The slurry would then undergo a particular water treatment process to remove contaminants from the water. After the contaminant is removed, the water would pass through a HGMS to remove the magnetite particles leaving a clean effluent. The induced flux on the filter is then shut off and the filter can be backwashed to recycle the particles.

Research objective

This research wishes to achieve high capture efficiencies for nanoscale magnetite particles. It looks to develop a basic understanding of the flow requirements required for high capture efficiencies of particles. By determining the flow requirements, the rate at which the particles can be removed will be deduced. This research also hopes to successfully capture magnetite particles dispersed with sodium tripolyphosphate and magnetite coated with silica. The capture of particles under these conditions will justify their further use. Additionally, this research looks to recapture a significant number of the particles. Recapturing the particles is absolutely critical to prove that they can be reused. By performing these bench scale filtration experiments, the overall feasibility of implementing this technology will be assessed.

Thesis structure

This thesis is divided into 5 different chapters. The first chapter is an introduction to the topic of HGMS. It establishes grounds for studying the HGMS of nanoscale magnetite by

exploring the use of nanoscale magnetite as an adsorbent of heavy metal ions. The introduction also provides alternative methods being examined for the removal of the particles to establish the principle differences in this technology and others. Chapter 2 is a literature review of HGMS. The literature review covers all the major components of previous HGMS research and development including theory, modeling, and experimental results. Chapter 3 covers the experimental setup, which describes the materials and apparatus used in this research and analytical methods used for the analysis of the results from filtrations. Chapter 4 presents the data obtained from filtrations and discusses the results as to explain trends and patterns present. Chapter 5 concludes the findings and discusses the degree that the objectives of this thesis have been achieved.

Chapter 2

Literature Review

The first section of this chapter describes the development of the basic principles and the characteristics associated with high gradient magnetic separators (HGMS). The second section describes the theory behind the capture of particles and different models created to simulate particle capture. The third section describes different experimental procedures and the results obtained from these filtrations.

The development of magnetic separation

Magnets have long been used to separate ferrous from nonferrous materials. A patent for a magnetic separator was awarded as early as 1792 in England for the separation of iron minerals (Gunther, 1909). Early attempts at magnetic separation were directed at strongly magnetic material, originally iron from brass filings and turnings, metallic iron from furnaces, and magnetite from gangue (Gunther, 1909). Like any other technology, crude machines lead the way to more sophisticated devices that could selectively and efficiently filter a variety of particles. Some major contributions to the development of magnetic separation are the invention of the electromagnet by William Sturgeon in 1825 (Bellis, 1997), inventions that impose magnetic forces on particles independent of path (Frantz, 1932, 1935), the use of high field intensity (Iannicelli, 1969), and the use of high field gradients (Kolm, 1971)

Early magnetic separation devices have a wide range of configurations; over 300 different patents exist in the United States alone (Gunther, 1909). Figure 2 below shows a drum-type separator one common configuration that demonstrates the principles behind early magnetic separation (Oberteuffer, 1974). Although this is just one configuration of a traditional magnetic separator, conceptually, they all work the same way. Magnetic separators apply a flux to a feed of particles and particles are routed in different directions based on their magnetic susceptibility.

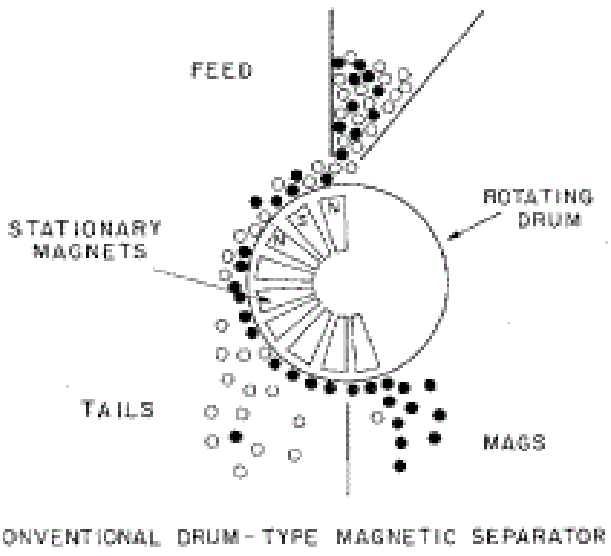

Figure 6. Example of a magnetic drum separator, (Oberteuffer, 1974).

As stated above, magnetic separation was initially limited to the separation of larger, highly magnetic materials. Since all materials are either attracted to or repelled by magnets, researchers and inventors began to develop more applications for separating materials by imposing magnetic forces on them. As the theory behind magnetic susceptibility developed, it was realized that localized points of magnetic fluxes limited both the capacity and sensitivity from which materials could be magnetically separated (Frantz, 1932). Samuel Frantz invented a device that placed a continual magnetic force on all the particles in the feed, which was nearly independent of each particles path, so each particle was equally and continually affected by the magnetic force (Frantz, 1932). By making the force placed on the particle virtually independent of path, the main limitations on the device were the velocity and magnetic susceptibility of the feed (Frantz, 1932). Frantz also noted that his machine could be run under wet and dry conditions. Although Frantz's invention did not create the high gradients across the entire cross-section of flow, which is characterized in modern magnetic separators, the main concept to make the magnetic force imposed on the particle independent of the particles path was essential in the development of HGMS. Frantz later incorporated a metal screen into the design for a magnetic separator creating even more similarities to modern day HGMS (Frantz, 1935).

Another major contribution to HGMS was the use of high intensity magnets to capture less magnetically susceptible particles (Iannicelli, 1969). Iannicelli noted that previous magnetic separation devices only applied the magnetic forces necessary to saturate iron. The magnetic

force is limited once the saturation of the material has occurred. Iannicelli (1969) deduced that by increasing the magnetic flux, additional minerals could be removed from clay slurries. Particularly, paramagnetic and diamagnetic materials since they require a larger field to be captured by HGMS.

The final major contribution is the development of high gradients, across the entire cross-section of the apparatus, to capture the particles (Kolm, 1971). Kolm noted that there are three major factors in magnetic separation: the magnetic flux, the competing forces, and magnetic field gradient (Kolm, 1971). Kolm (1971) mentioned that increasing the magnetic flux was only practical to a certain extent so examining the other aspects of separation would lead to superior HGMS devices. The next thing Kolm (1971) deduced in his patent was that the magnetic force was based on the size of the particle and therefore limited based on particular slurries. From this, he concluded that the best way to increase the efficiency of magnetic separation was to create a sufficient number of sites to capture all of the particles (Kolm, 1971). Although it is difficult to trace the major principles behind HGMS back to any source, these are three of the major achievements that led to modern HGMS.

The most common arrangement for modern HGMS consists of a column or tube containing a ferromagnetic material, typically steel wool, which is surrounded by electromagnets. A basic schematic for a HGMS is shown below in Figure 2 (Oder, 1976). This device has all of the principles stated above; it creates a continual magnetic force on each particle passing through the separator which increase the volume and precision at which particles can be captured, has a high intensity magnetic flux, and creates many field gradients. The magnetic gradient across the column is the main driving force for capture. The ferromagnetic material inside the column creates many field gradients to which particles can be attracted and attached. Stainless steel wool is an ideal material to pack a column with because of its large surface area to volume ratio, high magnetic susceptibility, and resistance to corrosion than other materials, such as carbon steel wool, that have been used in the past (Odder, 1976).

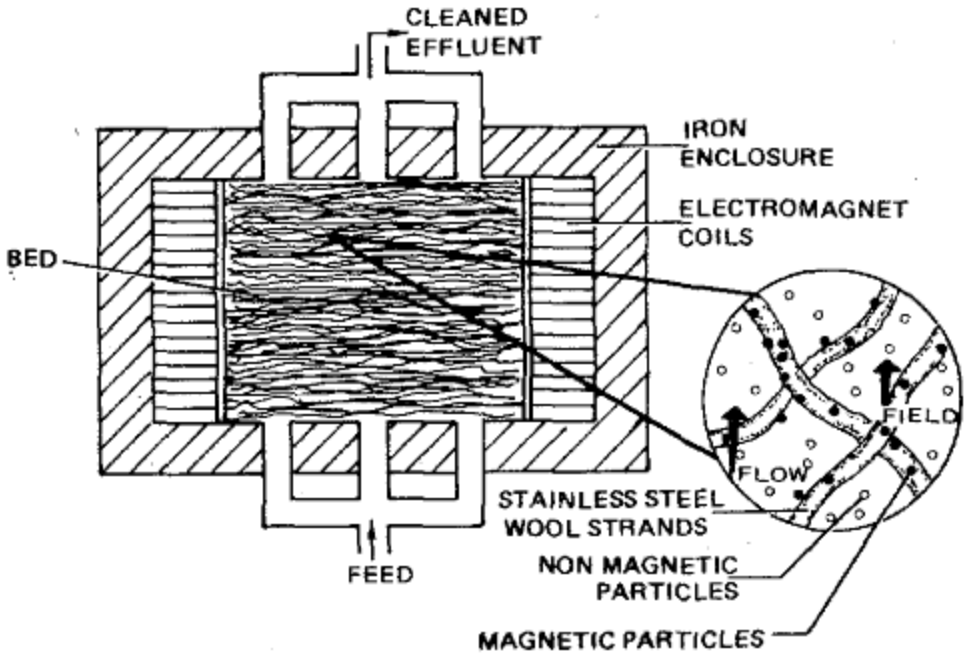

Figure 7. Schematic of a HGMS utilizing stainless steel wool as the magnetic media (R. R. Oder 1976)

HGMS theory and modeling

The theory behind HGMS separation is based on interacting forces. A given particles motion is dependent on all of the forces imposed on that particle. If the magnetic force can overcome the other forces acting on the particle it will be captured. The theory is derived by examining the capture on a single wire and expanding these concepts to circumstance with multiple wires. Particle size is also another factor that is widely examined and can be accounted for by including the most prominent forces present. The interacting forces are used to develop motion equations, and the motion equations are used to predict the capture efficiency of the separator.

This section will begin by giving an introduction to magnetism and move into the forces that are considered when modeling HGMS. Next, particle buildup considerations are reviewed. It will then move into the single wire theory. After that some of the performance models will be shown for both large particles and nano-scale particles. The final section will discuss the recovery of particles.

Magnetic field, magnetic induction, magnetization, and magnetic dipoles

Magnetic materials can be divided into four major groups: paramagnetic, diamagnetic, ferromagnetic, and superparamagnetic. In HGMS theory, paramagnetic and diamagnetic materials are often grouped together because they are distinguishable from the other groups in that their magnetization is directly proportional to the magnetic field, they are relatively weakly magnetic, have no coercivity, and do not retain their magnetism (Scott, 1959; Bleaney, 1989; Gerber, 1983; Ebner, 1997). Conversely, the magnetization of ferromagnetic materials is not proportional to the magnetic field, is relatively high, and remains after the field is removed (Scott, 1959). Superparamagnetic materials act similarly to ferromagnetic materials but they lack coercivity (Moeser, 2002). Nano-scale ferromagnetic materials exhibit superparamagnetic properties (Moseser, 2002).

Paramagnetic materials

Typically, magnetic field vectors are expressed in terms of magnetic induction or flux field *B* and magnetic field strength *H* (Scott, 1959; Bleaney, 1989; Ebner, 1997). The *B* and *H* fields are related in the following equations where μ_m is the magnetic permeability (Scott, 1959; Bleaney, 1989; Ebner, 1997).

$$B = \mu_m H \tag{2}$$

When a paramagnetic material is in the presence of a magnetic field, the material becomes magnetized to a magnetization *M* (Scott, 1959; Ebner, 1997). The magnetization can be related to the *H* field in the following equation where χ_m is the magnetic susceptibility of a material (Scott, 1959, Ebner, 1997).

$$M = \chi_m H \tag{3}$$

Equation 1 can also be written in the following ways to relate the *B* and *H* field to χ_m *and* *M* since $\mu_m = \mu_o(1+\chi_m)$ where μ_o is the permeability of free space (Scott, 1959; Ebner, 1997).

$$B = \mu_o(1 + \chi_m)H \tag{4}$$

$$B = \mu_o(H + M) \tag{5}$$

The force that a magnetic field induces on a dipole is known as the as Lorentz Force (Scott, 1959). Two examples of dipoles are closed loops and bar magnets (Ebner, 1997). The force can be defined by the following equation where *q* is the electric charge of the particle, *v* is the instantaneous velocity of the particle, and *B* is the magnetic induction (Scott, 1959; Ebner, 1997).

$$F = qv \times B \tag{6}$$

Similarly, the torque τ exerted on a wire loop with area *A* and current *I* can be expressed in the following equation where $\hat{\mu}$ is the magnetic dipole and $|\hat{\mu}| = IA$. The vectors direction depends on the right hand rule (Scott, 1959; Ebner, 1997).

$$\tau = \hat{\mu} \times B \tag{7}$$

The potential energy can then be denoted with the following equation (Ebner, 1997).

$$U = \hat{\mu} \cdot B \tag{8}$$

Ferromagnetic materials

Ferromagnetic materials act differently than paramagnetic and diamagnetic materials. This is due to the fact that ferromagnetic materials act in a nonlinear fashion and their magnetization is related to previous magnetization of the material (Scott, 1959). When magnetizing ferromagnetic particles, any previous magnetization will give preference to the original direction of magnetization (Scott, 1959). Additionally, the magnetization of the material will result in residual magnetism (Scott 1959). This relationship can be seen in the following plot of the *B* and *H* field, denoted as a hysteresis loop.

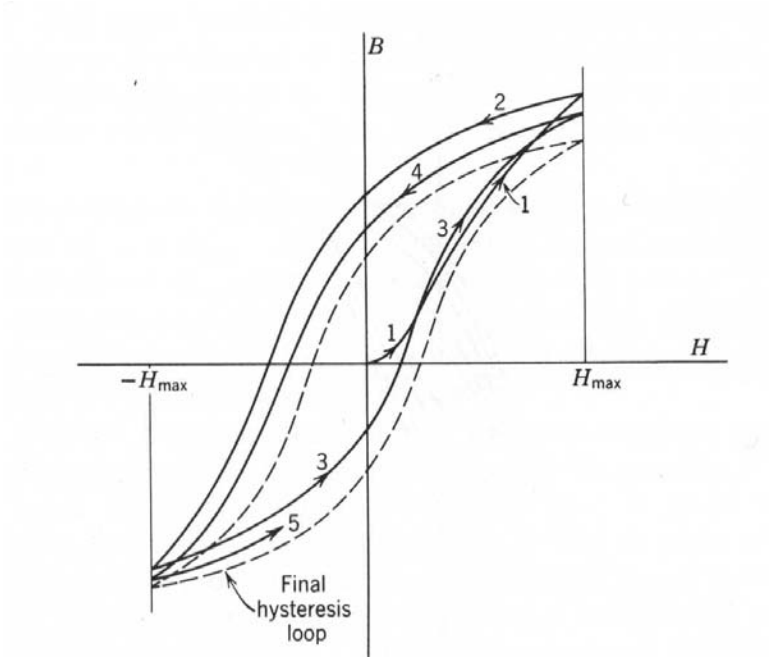

Figure 8. Hysteresis loop, (Scott, 1959)

For a ferromagnetic material with no initial induction or field, which can be achieved with heat treatment, the curve would begin at the origin of the graph (Scott, 1959). Upon increasing the magnetic field *H* to a constant value H_{max}, the *B* field would increase nonlinearly to a value following curve 1 (Scott, 1959). Removing the implied field *H* will result in a residual magnetic induction *B* (Scott, 1959). If the *H* field is then reverse, the polarity of the field will decrease further, pass through zero, and obtain a new *B* field following curve 2. Likewise, a change in the implied field to the positive H_{max} will reverse the polarity of the *B* field again resulting in a slightly different maximum induction. If this process is repeated about 20 to 30 times a final hysteresis loop, denoted by the dashed line, will be reached (Scott, 1959).

It is also useful to plot hysteresis curves for varying implied fields, doing this will result in the following graph.

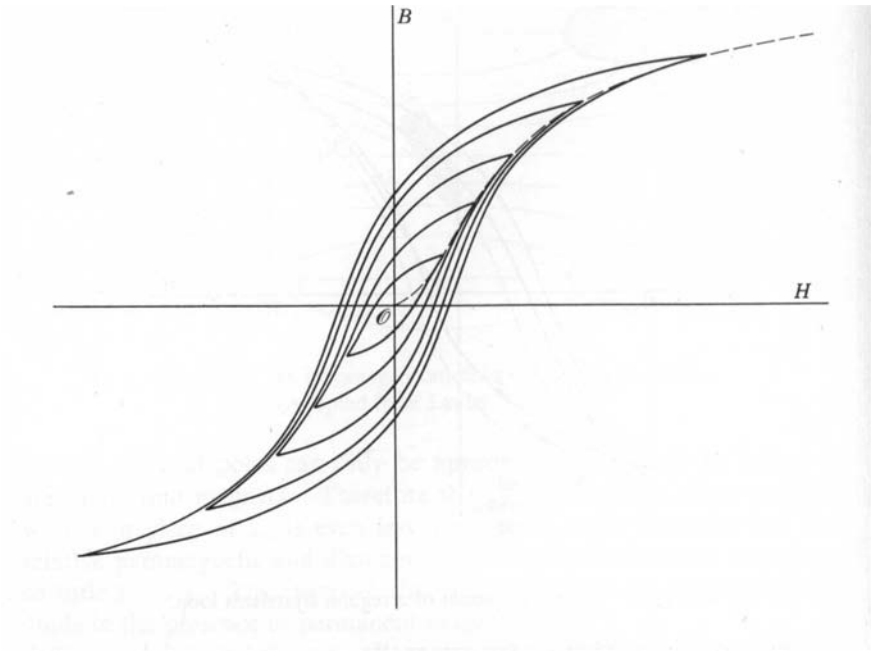

Figure 9. hysteresis curves for various implied fields, (Scott, 1959)

As can be seen, hysteresis curves are repeatable and follow a trend. The dotted line through each individual value of H_{max} represents how the B increases with H. There are two points that are particularly important on each hysteresis loop, the $|B|$ for $H = 0$ defined as the residual induction B_r,and $|H|$ for $B = 0$ or the coercive force H_c (Scott, 1959). Additionally, it should be observed that as the loops become larger the curve going through H_{max} of each individual curve begins to flatten out. As the line straightens out, it will reach an upper limit of the form $B=\mu_o(H+M_{sat})$, where M_{sat} is the saturation magnetization (Scott, 1959). M_{sat} is constant and represents the maximum possible magnetization of a given material (Scott, 1959). The residual induction and the coercive force are often taken to be for the maximum hysteresis curve (Scott, 1959).

Due to the nonlinear nature of the magnetization of ferromagnetic materials, the magnetization of the particles being captured is usually assumed to be saturated to model the behavior or strongly magnetic particles (Takayasu, 1983). In this case, the magnetization of the particle will replace χH (Takayasu, 1983).

Superparamagnetic materials

Superparamagnetic materials are ferromagnetic particles that are small enough that they can be considered a single domain and the surrounding temperature is large enough to equilibrate any residual magnetism (Bean, 1955). So like ferromagnetic materials, superparamagnetic materials have a very large magnetic moment that does not increase proportionally to the field (Bean, 1955; Moeser, 2002). Conversely, the particles are small enough that when the magnetic field is removed the particles do not hold any magnetism or have no coercive force (Moeser, 2002). The consequences of this can be observed in Moeser findings in *Water-Based Magnetic Fluids as Extract ants for Synthetic Organic Compounds*. In this study, Moeser induced a field across different weight fractions of nano-scale magnetite solutions and it can be seen that increased loadings of particles increases the magnetization of the fluid and the fluid becomes saturated, see the figure below (Moeser, 2002).

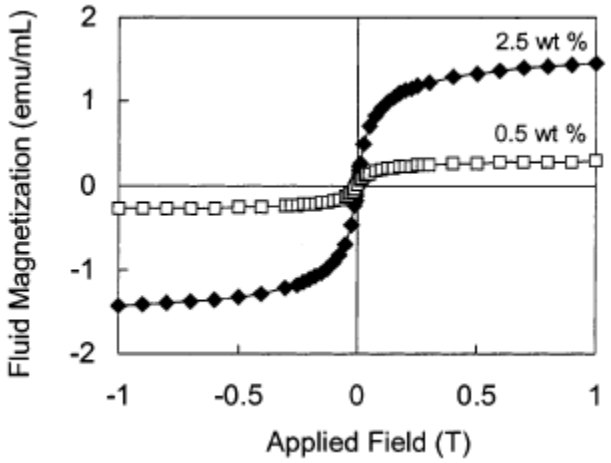

Figure 10. Magnetization response of a nano-scale magnetite solution for various weight concentration loadings, (Moeser, 2002).

Moeser's separation theory makes the assumption that the magnetite core of his particle is saturated (Moeser, 2004). By making this assumption, equations can be developed to determine the particle capture efficiency (Moeser, 2004). Another paper (Takayasu, 1983) uses two equations to calculate the magnetization M_p of submicron sized magnetite where M_{sp} is the saturation concentration, V is particle volume, k is the Boltzmann constant, and T is the absolute temperature.

$$M_p = M_{sp}\left\{\coth\left(\frac{VM_{sp}H_o}{kT}\right) - \frac{kT}{VM_{sp}H_o}\right\} \tag{9}$$

For the case where $VM_{sp} >> kT$ the magnetization M_p is given by the following equations (Takayasu, 1983).

$$M_p = \begin{cases} M_{sp}, \left(H_o \geq M_{sp}/3\right) \\ 3H_o, \left(H_o < M_{sp}/3\right) \end{cases} \tag{10}$$

Competing forces

The principle behind the HGMS of particles is based on competing forces. The major forces imposed on particles associated with HGMS are as follows magnetic, drag or viscous, diffusion, and gravitational (Gerber, 1984, Fletcher, 1991). The interactive forces are Lifshitz-van der Waals, electrostatic double layer, hydration, and magnetization (Rebodos, 2010). All of these forces can be added in order to formulate the net force on a particle. Often some of these forces are neglected or combined in order to simplify the equation. The following paragraphs will further describe these forces which will lead to equations that determine the capture efficiency of a filter. Typically, forces are derived and then converted into polar coordinates in order to develop trajectory models for flows perpendicular to wires (Watson, 1973; Cotton, 2002; Ebner, 2001; Fletcher, 1991; Clarkson, 1976; Birss, 1978; Moeser, 2004; Gerber, 1983). Additionally, cases with flow parallel to the wire (Gerber, 1983; Uchiyama, 1976) and at an angle with the wire (Sheere, 1981). Also, most models are adapted for paramagnetic or diamagnetic models (Watson, 1973; Akoto, 1977; Gerber, 1983; Gerber, 1984, Fletcher, 1991; Tsukamoto, 1995; Ebner, 1997; Luborsky, 1975; Sheerer, 1981). Other models are designed for ferromagnetic and parasitic ferromagnetic (Takayasu, 1983; Uchiyama, 1976; Gerber, 1996), both paramagnetic and ferromagnetic (Clarkson, 1976), and superparamagnetic (Moeser, 2004,; Ditsch, 2005). All models are designed for ferromagnetic wires within the filter, usually either wires, ribbon, or spheres.

The magnetic force

The magnetic force can be derived by taking the gradient of the magnetic energy U where $\chi = \chi_p - \chi_f$ is the difference of the susceptibility of a paramagnetic particle and the fluid , V_p is the volume of the particle (Watson, 1973; Gerber, 1983; Takayasu, 1984; Ritter, 1997; Cotton, 2002; Ebner, 1997).

$$\vec{F}_m = \tfrac{1}{2}\mu_o \chi V_p \times \nabla(H^2) \tag{11}$$

The force exerted by the magnet on a particle has also been reported as follows for diamagnetic and paramagnetic particles (Fletcher, 1991).

$$\vec{F}_m = \mu_o \chi V_p H * \nabla(H) \tag{12}$$

The magnetic force is also derived to be the following for ferromagnetic and paramagnetic particles (Luborsky, 1975; Clarkson, 1976).

$$\vec{F}_m = \tfrac{1}{2} V_p \nabla(M_p H) \tag{13}$$

The following case is used for superparamagnetic particles (Moeser, 2004; Ditsch, 2005).

$$\vec{F}_m = \mu_o V_p M_p \cdot \nabla(H) \tag{14}$$

The viscous drag force

The viscous force can be derived from Stokes Law which can be written as follows where η is the dynamic viscosity of the fluid, r is the radius of a spherical particle, and $(\vec{v} - \vec{V})$ is the particle's velocity relative to the fluid's velocity (Watson, 1973; Clarkson, 1976; Gerber, 1983; Takaysu, 1984; Moeser, 2004).

$$\vec{F}_v = -6r\pi\eta(\vec{v} - \vec{V}) \tag{15}$$

The gravitational force

The following equation is that of the gravitational force of a particle in a fluid (Gerber, 1983).

$$\vec{F}_g = V_p \vec{g}(\rho_p - \rho_f) \tag{16}$$

The diffusion equation

One method for representing diffusion is by establishing a time rate change of concentration of particles about a wire and using this equation to develop a steady state concentration of particles being captured (Takayasu, 1983). The following equation represents such a change in concentration where $D=kT/(6\pi\eta b)$ is the diffusion coefficient, , η is the viscosity fluid, k is the Boltzmann constant, T is the absolute temperature, b is the particle radius, and v is the terminal velocity obtained from setting $F_m=F_v$ (Takayasu, 1983; Fletcher, 1991).

$$\frac{\partial c}{\partial t} = D\nabla^2 c - \nabla \cdot (vc) \tag{17}$$

Fletcher's *Fine Particle High Gradient Magnetic Entrapment* uses the steady state solution of the concentration rate change equation to develop an equation for the "force" that diffusion imposes on particles as follows (Fletcher, 1991).

$$F_{dr} = -\frac{kT}{n}\frac{dn}{dr} \tag{18}$$

$$F_{d\theta} = -\frac{kT}{n}\frac{1}{r}\frac{dn}{d\theta} \tag{19}$$

Interactive forces

The interactive forces can be expressed in terms of the potential energy present (Rebodos, 2010). Generally if the total potential energy is positive, the suspension is stable. If the total potential is negative, the suspension is instable or the particles have a tendency to aggregate. The following equation can represent the total potential energy present U_T where U_{vdW}, U_{ES},

U_{AB}, and U_M represent the Lifshitz-van der Waals, the electrostatic double layer, the hydration, and the magnetization energies (Rebodos, 2010).

$$U_T = U_{vdW} + U_{ES} + U_{AB} + U_M \tag{20}$$

The interactive force can be incorporated into HGMS through the diffusion equation (Gerber, 1984; Fletcher, 1991). The major forces considered in this case are the hydrodynamic, electrostatic double layer, and the magnetic force (Gerber, 1984; Fletcher, 1991). Lifshitz-van der Waals force is not considered in this case because it occurs at a relatively short range compared to the others and is considered after adsorption takes place (Fletcher, 1991). When taking hydrodynamic forces into account, D and η become a function of c. Equation 15 can be altered to account for this change where $r_a=r/a$ or the position of the particle divided by the radius of the wire (Gerber, 1984).

$$\frac{\partial c}{\partial t} = \frac{\partial}{\partial r_a}\left[(1+1.45c)\frac{\partial c}{\partial r_a} - G(r_a)(1-6.55c)c\right] \tag{21}$$

The electrostatic force and magnetic forces are incorporated into the diffusion equation differently by modifying the temperature term in the "diffusion force" (Fletcher, 1991). The following two expressions are derived from the energy equations of the electrostatic force and magnetic force where T_{DL}, ε_o, ε_r, ψ_o, and k represent the temperature associated with the electrostatic force, the absolute and relative permittivity of the liquid, the double layer potential, and Debye-Huckel parameter and T_{DD}, B_o, and b represent the temperature associated with the magnetic interaction, the background field, and the particle diameter, respectively (Fletcher, 1991).

$$T_{DL} = \left(\frac{8\pi}{3}\right)\frac{\varepsilon_o\varepsilon_r\psi_o^2}{9\eta b}\left(\frac{3c}{4\pi}\right)^{2/3}\partial r \tag{22}$$

$$T_{DD} = \left(\frac{16\pi}{9\mu_o}\right)\frac{\chi B_o^2 b^2}{k}\left(\frac{3c}{4\pi}\right)^{4/3}\partial r \tag{23}$$

These equations can then by substituted into the force equation for diffusion by setting $T^*=T+T_{DL}+T_{DD}$ as follows (Fletcher, 1991).

$$F_d = -\frac{kT^*}{n}\nabla n \tag{24}$$

Particle buildup

As particles buildup they affect the capture efficiency of the filter. Theories for the buildup of particles on a singular wire have been developed for paramagnetic (Luborsky, 1976; Friedlaender[2], 1981; Hollingworth, 1984) and superparamagnetic particles (Moeser, 2004; Ditsch, 2005). By examining the particle buildup on HGMS elements, the theory is more complete and accurate. Additionally, the saturation buildup can be determined which is useful when determining when to backwash the filter.

The particle trajectory towards a given object can be calculated as shown previously, considering the most prominent force equations for a given scenario (Luborsky, 1976). After determining the trajectories of particles, the forces exerted on each layer of particles can be determined given the particle size (Luborsky, 1976). The critical point of buildup occurs when the magnetic force can no longer hold the particles. This occurs when the tangential component of the viscous drag forces is greater than the tangential force component of the magnetic force (Luborsky, 1976). Another important thing to consider is the zone where the particles are to be captured. This can be defined by again examining the trajectories of particles and solving for the specific case when the radial component of the magnetic force $F_{mr}=0$ (Friedlaender[2], 1981). This curve is a function of the magnetic velocity $K_s=M/(3H_o)$ and the normalized position $r_a=r/a$ as defined by (Friedlaender[1], 1981). The following equation describes the particle buildup curve θ_c on a spherical magnetized object (Friedlaender[2], 1981).

$$|\theta_c| = \arcsin\left[\frac{2(1+2K_s r_a^{-3})}{3(1+K_s r_a^{-3})}\right]^{\frac{1}{2}} \tag{25}$$

The accumulation of particles will occur and will continue while the following two parameters hold true where F_g are the components of the gravitational force (Friedlaender[2] 1981).

$$F_{mr} + F_{gr} \leq 0 \tag{26}$$

$$F_{m\theta} + F_{g\theta} + F_{d\theta} \leq 0 \tag{27}$$

The following figure shows a picture of the completed model for the buildup on a spherical particle.

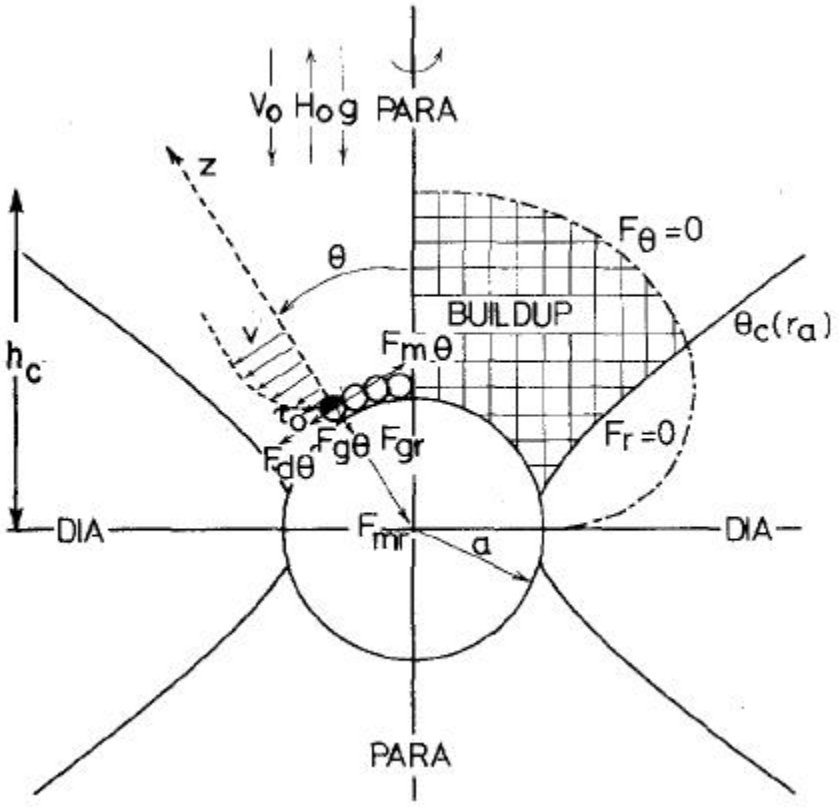

Figure 11. Buildup model schematic, (Friedlaender[2], 1981).

The static buildup limitation for superparamagnetic particles was developed and incorporated into a performance equation by Moeser and Ditsch. Incorporating buildup into the performance equation allows for a more dynamic approach to determining the effectiveness of filters.

HGMS performance evaluation

There are two major methods to evaluate the performance of a filter. One method is trajectory based (Watson, 1973; Lubrosky, 1975; Clarkson, 1976; Uchima, 1976; Birss, 1978; Gerber, 1983;) and the other is based on static buildup limitaitions (Fletcher, 1991; Moeser, 2004; Ditsch, 2005). The former case was developed for larger sized particles under different flow and packing conditions in the case where diffusion was not a factor. The latter case was developed for smaller particles in which diffusion was considered to be significant when modeling the capture behavior. In both cases the models are developed based on a force balance. A trajectory based model develops motion equations, while a static buildup model determines the limitations of buildup based the limitations that the forces impose.

Trajectory based

Watson's *Magnetic Filtration* develops a capture efficiency equation by examining an element of a magnetic filter with thickness *dx*, particle loading *N*, fluid velocity V_o, and magnetic field H_o (Watson, 1973). The figure below illustrates the single element of a filter originally produced by Watson in *Magnetic Filtration*.

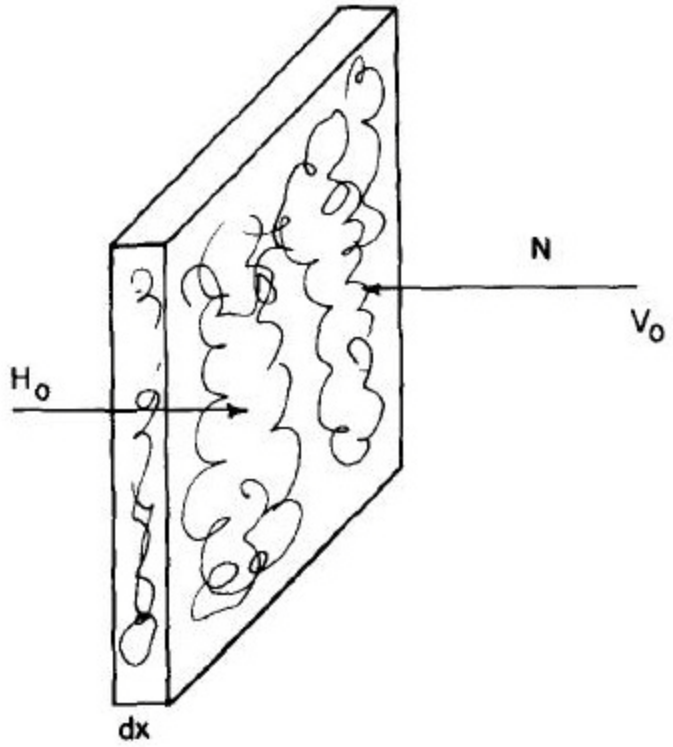

Figure 12. An element of a magnetic filter with thickness *dx*, field strength H_o, particle loading *N*, and fluid velocity V_o, (Watson, 1973).

Then by looking at one fundamental element of the filter, or a single wire, a motion equation can be developed for a particle passing by the individual wire (Watson, 1973). The coordinate system used in Watson's *Magnetic Filtration* is defined below.

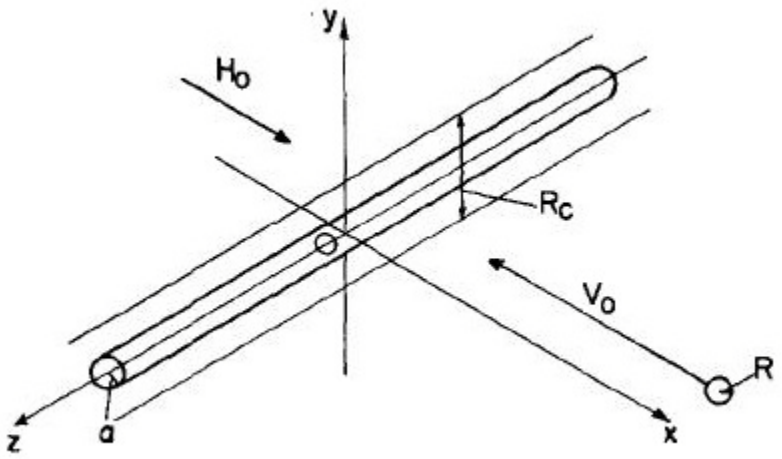

Figure 13 Coordinate system containing a ferromagnetic wire of radius *a*, magnetic field of H_o, fluid velocity V_o, particle radius *R*, and radius of capture R_c, (Watson, 1973).

Watson then developed the following motion equation based on magnetic and viscous drag forces for a paramagnetic particle given in the above coordinate system (Watson, 1973).

$$\frac{dr_a}{dt} = \left(\frac{V_o}{a}\right)\left(1-\frac{1}{r_a^2}\right)\cos\theta - \left(\frac{V_m}{a}\right)\left(\frac{M_s}{2\mu_o H_o}\right)\frac{1}{r_a^5} - \left(\frac{V_m}{a}\right)\frac{\cos 2\theta}{r_a^3} \tag{28}$$

$$r_a\frac{d\theta}{dt} = -\left(\frac{V_o}{a}\right)\left(1+\frac{1}{r_a^2}\right)\sin\theta - \left(\frac{V_m}{a}\right)\frac{\sin 2\theta}{r_a^3} \tag{29}$$

Where

$$\left(\frac{V_m}{a}\right) = \frac{2}{9}\left(\frac{\chi M_s H_o R^2}{\eta a^2}\right) \tag{30}$$

In the above equation, the ferromagnetic wire is assumed to be magnetized to a saturated value of M_s placed axially along the z axis, as shown in figure 8. The particle is paramagnetic with susceptibility of χ, volume of $V_p=4/3\pi R^3$, and density ρ_p. The fluid velocity V_o is uniform in the x direction with viscosity η. Additionally, r_a is defined as r/a and $\mu_o = 4\pi*10^7\ Hm^{-1}$ is the

permeability of a vacuum. These equations were solved numerically and it was found that the capture cross section per unit length of wire $2R_c$ was proportional to V_m/V_o, where V_m is the magnetic velocity and V_o is the initial velocity as seen below (Watson, 1973).

$$R_c \propto 1/2\left(V_m/V_o\right) \tag{31}$$

The filter performance was then determined for a filter of length L and filling factor F, which represents the length of wires in a given cross section that will affectively intercept particles from the flow, as follows where N_{out} and N_{in} are the number of particles leaving and entering the filter (Watson, 1973).

$$\frac{N_{out}}{N_{in}} - 1 = \exp\left(-\frac{4FR_cL}{3\pi a}\right) - 1 \tag{32}$$

Watson utilizes the developed model to determine the removal efficiency of waste water floc containing paramagnetic Fe_2O_3 particles (Watson, 1973). He considers a stainless-steel wool filter with radius of a=12μm and saturation magnetization of M_s=0.2 T (Watson, 1973). The applied magnetic field is H_o=1.19*10^6 A/m. Then it is assumed that the floc particles have a radius R=25μm containing 10 % Fe_2O_3 with average susceptibility of χ=7*10^{-4} (Watson, 1973). The viscosity of the water was selected to be η=1*10^{-3}kg/m sec and F~1% (Watson, 1973). The filter is considered to be 1 cm long (Watson, 1973). Watson considers the time required to fill the void space of the filter. Since the time is significantly low, he calculates a value V_{ex} the material extracted magnetically by setting the equal and opposite to each other (Watson, 1973). The results to his calculations can be seen in the table below (Watson, 1973).

Table 2 Capture efficiency of a floc containing Fe_3O_2 particles, reproduced from Watson's *Magnetic Filtration*.

V_0 (m/sec)	V_m/V_0	R_c	N_0/N_i [a]	T_f [b] (sec)	V_{ex} [c]
0.045	40	4.15	4×10^{-7}	10^3	33.6%
0.18	10	2.39	2×10^{-4}	2.8×10^2	11.4%
0.45	4	1.55	4×10^{-3}	1.1×10^2	4.8%

[a] Calculated for 1 cm thickness of filter.
[b] T_f time to extract material equal to the filter void space if fluid contains 2% solid matter; $V_m/a = 1.49\times10^5$ sec^{-1}.
[c] $V_{ex} = \pi F[(V_m/V_0)^{2/3} - 1]$.

Static buildup based model

Moeser's static build up limitation model considers a filter with wires of radius *a* orientated perpendicular to an applied magnetic field with a fluid flow perpendicular to the wire and magnetic field as shown in the figure below (Moeser, 2004).

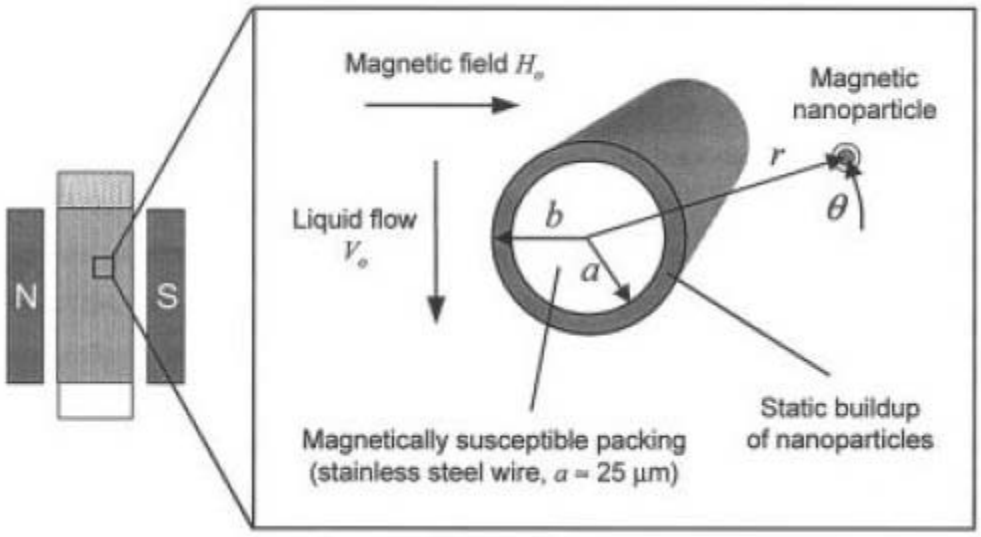

Figure 14. HGMS model schematic of a nano-scale magnetite particle coated with a nonmagnetic polymer, (Moeser, 2004).

Moeser's model uses a static balance around the wire to determine the radius at which a stable build up will occur (Moeser, 2004). The particles in the model are superparamagnetic nano-scale magnetite coated with nonmagnetic polymers (Moeser, 2004). The forces considered

in this model are fluid drag, diffusion from (Fletcher, 1991), and the magnetic force. From the summation of these forces, equal to zero assuming mass times acceleration is negligible, the following trajectory equations are obtained in the fluid around the static build region up where r_a is *r/a*, *n* is the number of particles, *G* is a geometry factor, and M_{wire} is the magnetization of the wire (Moeser ,2004).

$$\frac{dr_a}{dt} = -\tau_v G^- \sin\theta - \tau_d \frac{1}{n}\frac{dn}{dr_a} - \tau_m \left(\frac{M_{wire}}{2H_o r_a^5} + \frac{\cos 2\theta}{r_a^3} \right) \tag{33}$$

$$r_a \frac{d\theta}{dt} = -\tau_v G^+ \cos\theta - \tau_d \frac{1}{r_a n}\frac{dn}{d\theta} - \tau_m \frac{\sin 2\theta}{r_a^3} \tag{34}$$

The constants τ_v, τ_d, and τ_m represent the fluid drag force, diffusion, and magnetic force, respectively as defined below where R_{core} is the radius of the particle core and R_{shell} is the radius of the entire particle (Moeser, 2004).

$$\tau_v = \frac{V_o}{a} \tag{35}$$

$$\tau_d = \frac{kT}{6\pi\eta R_{shell} a^2} \tag{36}$$

$$\tau_m = \frac{2\mu_o M_{wire} M_{core} R_{core}^3}{9\eta R_{shell} a^2} \tag{37}$$

The geometric factors were determined using Taylor series expansion to be as follows where *Re* is the Reynolds number (Moeser, 2004).

$$G^- = 0 \tag{38}$$

$$G^{+} = \frac{2R_{shell}/b}{2 - \ln \mathrm{Re}} \tag{39}$$

By solving the motion equation for two cases where diffusion was the limiting force of particle capture and where drag was limiting, dimensionless relationships were established for diffusion limit K_{md} and the drag limit K_{mv} as follows (Moeser, 2004).

$$K_{md} = \frac{\tau_m}{\tau_d} = \frac{4\pi\mu_o M_{wire} M_{core} R_{core}^3}{3kT} \tag{40}$$

$$K_{mv} = \frac{\tau_m}{\tau_v}\frac{a}{R_{shell}} = \frac{2\mu_o M_{wire} M_{core} R_{core}^3}{9\eta R_{shell}^2 V_o} \tag{41}$$

The above terms are similar to Watson's ratio of magnetic velocity to viscous drag velocity. These equations are used to determine if a given particle is likely to be captured or not (Moeser 2004). The greater the ratio, the more likely the particle will be captured (Moeser, 2004). Moeser then developed the following graph relating the velocity of the fluid V_o to the K_{md} and K_{mv} ratios as seen below based on a wire of radius a=25μm,an implied field of H_o=1 T, a core radius of R_{core}=3.25nm, a core magnetization of M_{core}=63emu/g, and a particle radius of R_{shell}=13nm (Moeser, 2004).

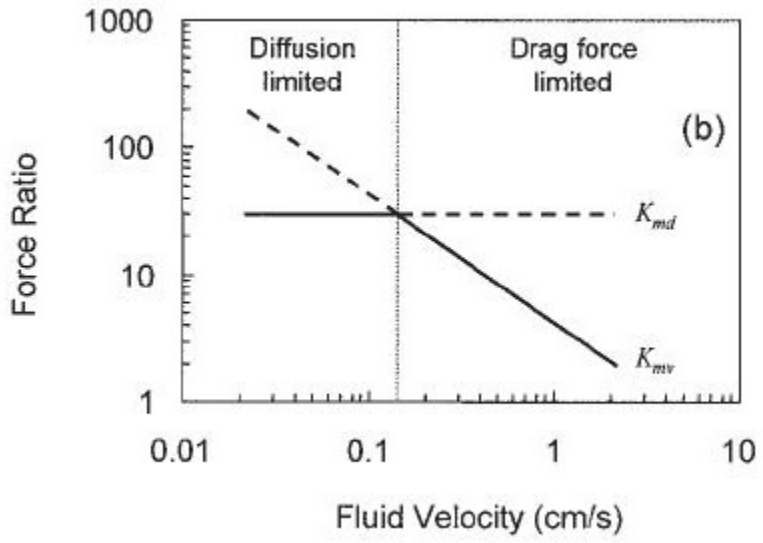

Figure 15. The effect of flow velocity on magnetic force ratios to diffusion and viscous drag, (Moeser, 2004).

The graph indicates two distinct regions: the diffusion limited region and drag force limited region (Moeser, 2004). In the former region, the diffusion controls the likely-hood of particles being captured because the magnetic force dominates the drag force (Moeser, 2004). As the velocity increases, the drag force begins to increase and then begins to become more significant than diffusion and eventually dominates the magnetic force (Moeser, 2004).

The preceding theory was then used by Ditsch to develop a capture efficiency model for a column of length *L* (Ditsch, 2005). Ditsch began by developing the following equation for the open volume of the column ϕ as follows where ϕ_i is the initial volume and *B* represents the volume of particles that have built up in the filter (Ditsch, 2005).

$$\phi = \phi_i - B \tag{42}$$

This expression can then be further developed into a parameter that describes the fraction of the column that has active wires (Ditsch, 2005).

$$F_C = \frac{(1-\phi_i)}{2} \tag{43}$$

In the previous equation, a factor of 2 is used to estimate the effects of the random orientation of the wires in the matrix (Ditsch, 2005). Given that the area to the wire cross section is A/π, the fraction of the column within the capture zone A_c is established as follows (Ditsch, 2005).

$$A_c = \frac{A}{\pi}\frac{(1-\phi_i)}{2} - B \tag{44}$$

From this, the fractional capture C is calculated as follows (Ditsch, 2005).

$$C = \frac{A_c}{\phi} = \frac{\frac{A}{\pi}\frac{(1-\phi_i)}{2} - B}{\phi_i - B} \tag{45}$$

The equation above is for the capture of particles in a single stage (Ditsch, 2005). In order to relate this expression to the total amount of particles captured, a particle number balance is completed for the following number density along the column where L is the height of the theoretical plate (Ditsch, 2005).

$$\frac{\partial n_o}{\partial x} = -\frac{n_o C}{L} \tag{46}$$

In general this expression cannot be solved as it is but when diffusion is not considered and the wires are clean, C becomes constant and reduces to the following form (Ditsch, 2005).

$$\frac{n_o}{n_{o,\,feed}} = \exp\left[-\frac{Cx}{L}\right] \tag{47}$$

The buildup of the wires can be represented in a separate equation. The following equation represents the change in build up over time where n_o is the number density of particles

far from the wire, n_s is the number density of particles in the buildup region, and V_o represents the open tube velocity (Ditsch, 2005).

$$\frac{\partial B}{\partial t} = \frac{n_o C}{n_s L} V_o \tag{48}$$

Particle recovery

The removal of particles from a HGMS is dependent on the surface interactions of the particles and the external forces, typically the shear, exerted on the particles (Svoboda, 1985). The different interactive energies considered by (Svoboda, 1985) are the electric double-layer energy U_R, Van der Waals potential U_A, magnetic dipole U_M, and hydrodynamic shear U_H. The total energy equation U_T can then be written by summing all of the interacting energies as follows (Svoboda, 1985).

$$U_T = U_R + U_A + U_M + U_H \tag{49}$$

The above relationship is a function of the mutual separation x, or the difference between a sphere and a flat plate as the formulas are derived and the pH of the solution (Svoboda, 1985). The following figure shows the U_T as a function of x with varying pH values (Svoboda, 1985).

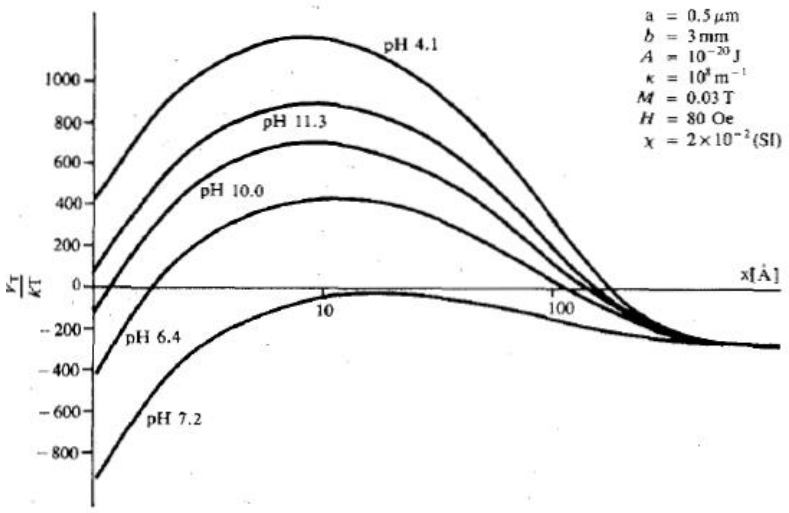

Figure 16. Total energy V_T versus the separation distance for varied pH values, (Svoboda, 1985).

The main point to take from the figure above is that at small distances U_T is approximately zero for pH of 11. Therefore, for the particular setup described above, the optimum pH to removal the particles from the matrix is 11 (Svoboda, 1985). These results are verified experimentally and will be discussed further in the next section.

Experimental research

HGMS has been researched in a variety of fashions in order to determine the feasibility of different applications and the accuracy of formulated models. Early experiments typically consisted of a single wire magnetized in a column with video cameras used to develop information about both the trajectory and ability of a wire to successfully capture both strongly and weakly magnetic particles of various sizes (Friedlaender, 1978; Schewe, 1980; Takayasu, 1980; Takayasu, 1983; Takayasu, 1984; Gerber, 1984; Gerber, 1996). Others have examined the HGMS of paramagnetic particles while passing through a random steel wool mesh (Oberteuffer, 1973), through multiple parallel wires (Uchiyama, 1976), and of ferromagnetic particles through a steel mesh (Leitermann, 1984). Recently, the examination of HGMS of nano-scale particles has been completed (Moeser, 2004; Ditsch, 2005; Yavuz[1], 2006; Yavuz[2], 2006). Experimental data is often given that shows the accuracy of the buildup area and the recovery of particles.

Trajectory analysis

Experimental procedure originally developed by (Friedlaender, 1978) and used by others (Schewe, 1980; Takayasu[2], 1983; Takayasu, 1984; Gerber, 1984) consisted of a television camera attached to a microscope that would videotape and take pictures of the collection process on a single wire (Friedlaender, 1978). Similar methods were used by (Takayasu, 1984; Gerber, 1996). By monitoring distance away from the wire in which particles were successfully captured radius R_c could be verified from previous theory over single element particle capture as seen in the following figure (Takayasu, 1984).

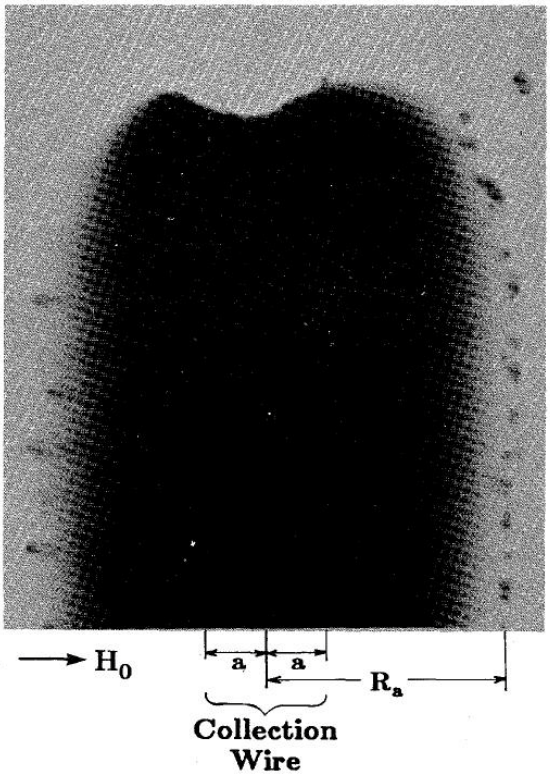

Figure 17. Capture of particles on a wire compared with the theoretical capture radius R_a, (Takayasu, 1984).

As can be seen above, the actual capture radius closely approaches the theoretical capture radius. The trajectory of the particle was determined through video images of particle motion to check the accuracy of a trajectory model, as is depicted in the figure below, where the circles represent the actual path of the particles, the solid line represents the calculated trajectory for laminar flow, and the dashed line represents the calculated trajectories for potential flow (Schewe 1980).

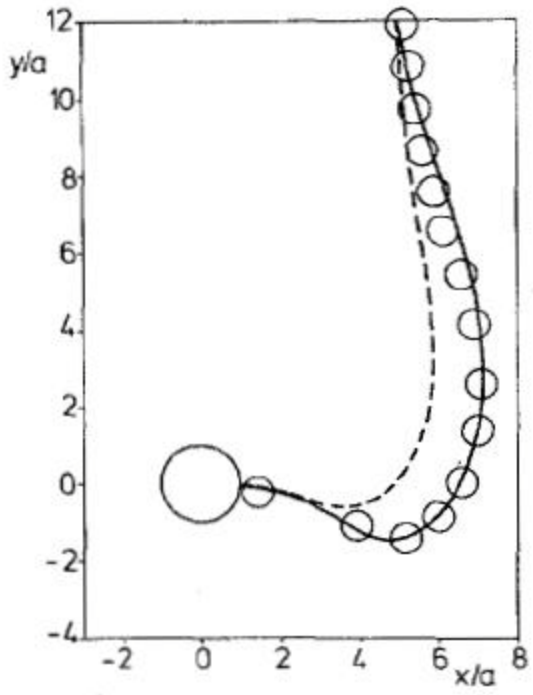

Figure 18. Experimental particle trajectory compared to actual particle trajectory, (Schewe, 1980).

Again the experimental data matches the theoretical data closely which indicates that for a single wire the theoretical equations are exceptionally accurate.

Nanoscale magnetite/magnetite-composite captures

The four most relevant papers to this research were completed by Moeser, Yavuz, and Ditsch. All four papers (Ditsch, 2005; Moeser, 2004; Yavuz[1], 2006; Yavuz[2], 2006) used a model L-1CN S.G. Frantz canister and a column packed with stainless steel wool. Moeser's column was 22.6 cm long and had a volume of 5.77 cm^3 (Moeser, 2004). The particles used were polymer coated and the diameter of the magnetite core was about 7.5 nm and with a total diameter was about 26 nm (Moeser, 2004). The following figure shows the fraction of the particles passing through column against the fluid volume on top compared to the theoretical capture limitations developed previously at a magnetism of 1.3 Tesla (Moeser, 2004).

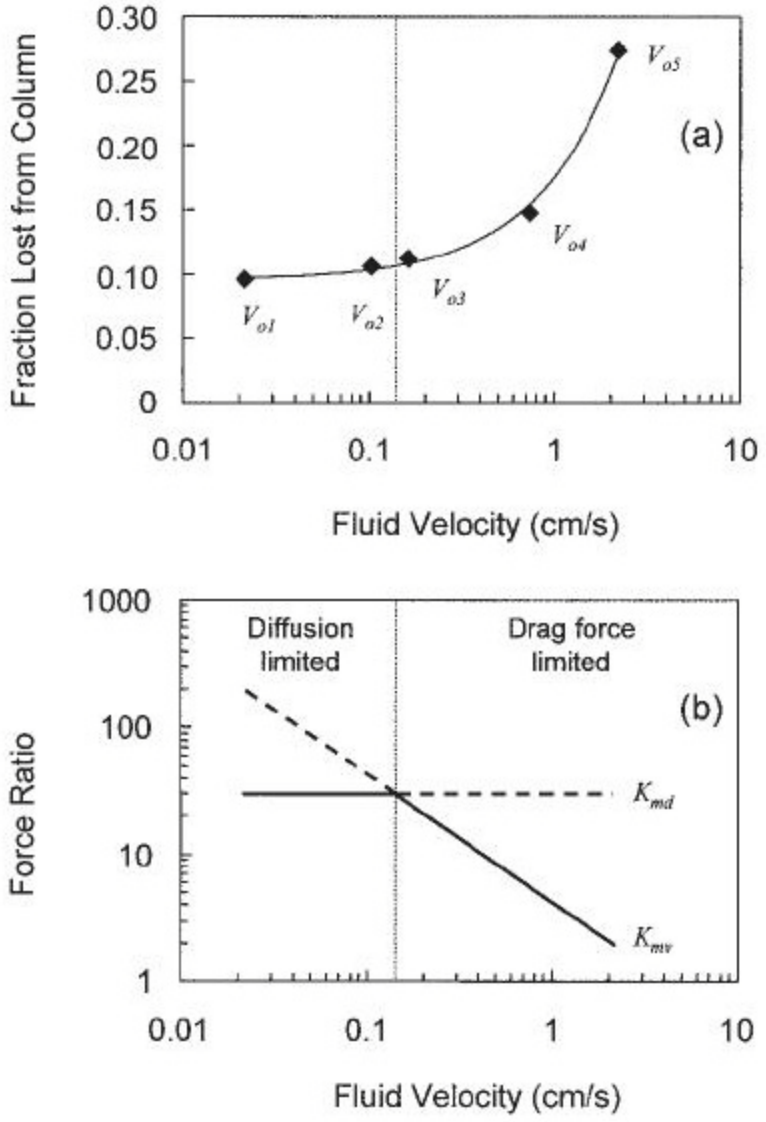

Figure 19. Capture efficiency of 8 nm polymer coated magnetite (above) compared to force limiting factors, (Moeser, 2004).

The capture efficiencies are a maximum at around 90 % and drops off relatively quickly as the drag force decreases (Moeser, 2004). Yavuz gravity fed particles of different sizes through a 22.3 cm long column and varied the strength of the magnetic field to determine the required field strength to remove the particles (Yavuz[2], 2006). The results from this study show that 20 nm particles are relatively easily captured, but as the size decreases the loss of retention drops off quickly (Yavuz[2], 2006). Figure A below represents the amount of particles retained

compared to the magnetic field, and figure B shows the optimum size of particle for capture and recovery of particles (Yavuz[2], 2006).

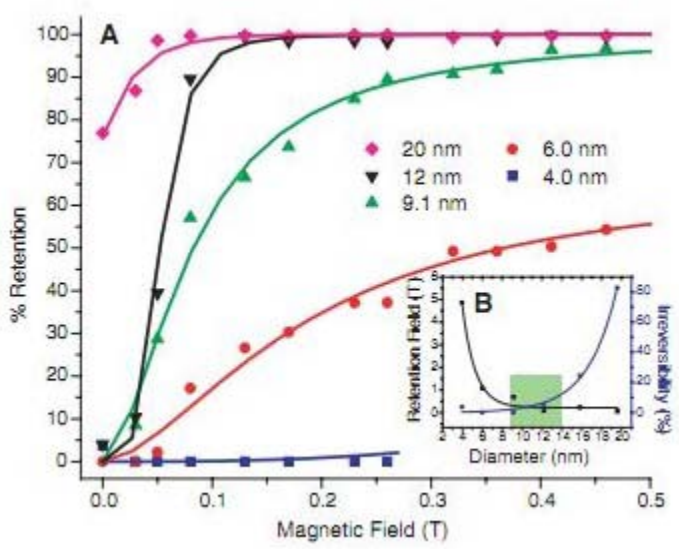

Figure 20. A) Retention of different sizes of magnetite particles for different magnetic fields B) The critical size for particles to be recovered, (Yavuz[2], 2006).

Ditsch used a 3.5 cm and a 10.5 cm long column to capture particles ranging in size from 80 nm to 140 nm under a magnetic field of 1.3 Tesla (Ditsch, 2005). Capture efficiencies for the 140 nm particles were greater than 99.9% at 1 cm/s (Ditsch, 2005). Refer to the following figure of the capture efficiencies versus the number of column volumes passing through the filter for different velocities, particle sizes, and column sizes (Ditsch, 2005).

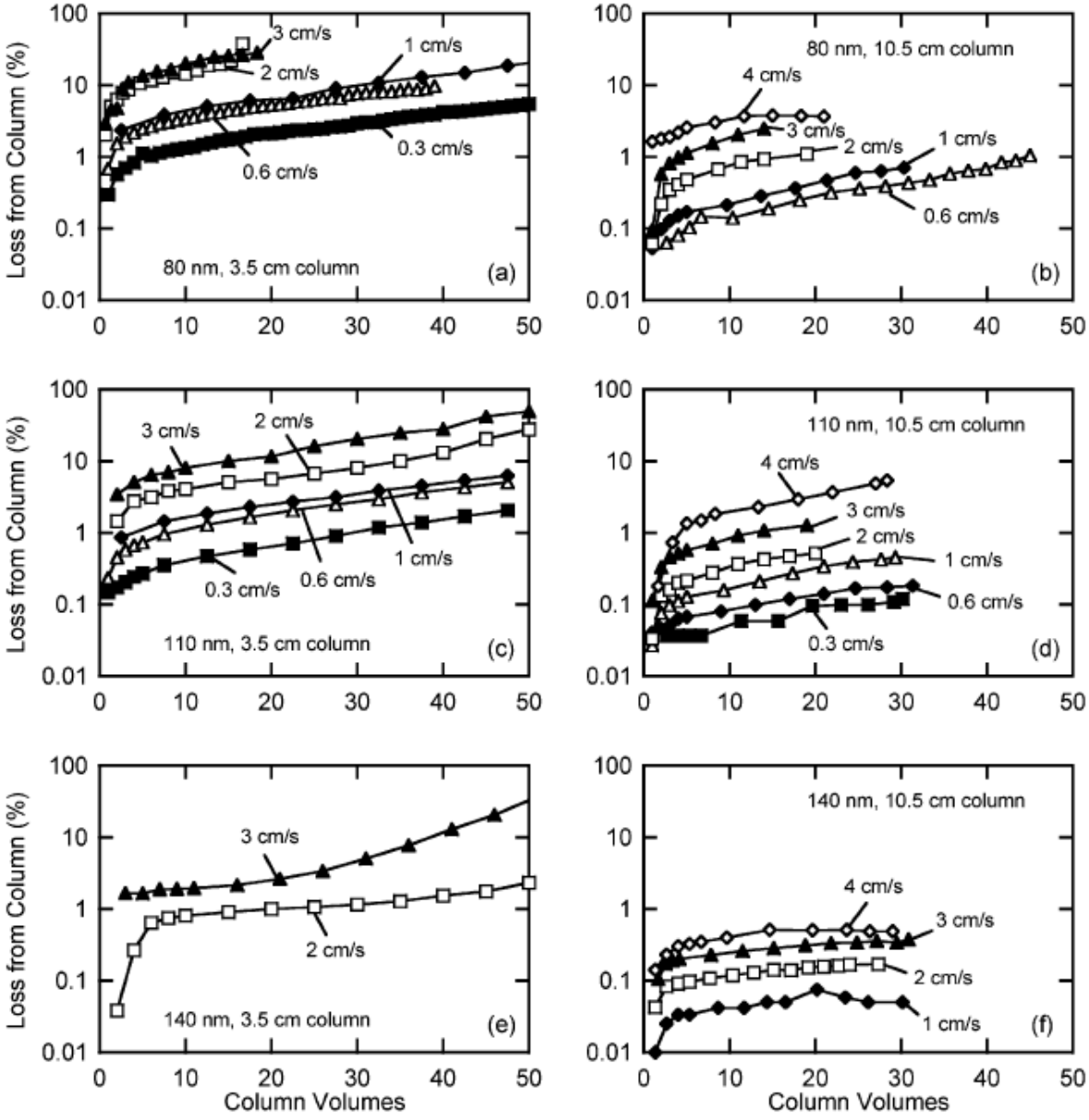

Figure 21. Loss from column over volumes through the column for varied particle sizes, velocities, and column sizes, (Ditsch, 2005).

It can be deduced from previous research that high capture efficiencies can be achieved. Yavuz's gravitation fed filter had the highest capture efficiency for magnetite particles of a small sizes around 100% for 20 nm particles at about 0.1 Tesla (Yavuz[2], 2006). Ditsch was able to achieve high particle removal efficiencies at a multitude of flowrates and for different column lengths but the particles were relatively larger than Moeser's or Yavuz's (Ditsch, 2005). Moeser was unable to achieve as high of particle captures even at a low velocity, most likely due to the

polymer coating and the size of the magnetite cores. Adding the polymer coating increases the stability of the particle. Having a smaller core, around 7.5 nm, decreases the force induced on the particle by the magnet.

Chapter 3

Experimental Materials and Methods

Experimental materials

Commercial grade nanoscale magnetite particles provided by Nanostructured & Amorphous Materials, Inc. were used. The particles in solution ranged from 15 to 20 nm determined by direct light scattering of the supernatant of the magnetite water solution. Silica-coated commercial magnetite particles as well as silica magnetite composites were used. Both the silica-coated commercial magnetite particles and silica magnetite composites were synthesized by Damber Hamel. The silica to magnetite mole ratio for the silica coated and composite particles was 3.48 and 4, respectively. Dispersed experiments utilized sodium tripolyphosphate ($Na_5P_3O_{10}$) to stabilize the particle suspension. A dispersant creates surface conditions on the particle that prevent aggregation and also cause the particles to become hydrophobic. Magnetite can be synthesized through a precipitation reaction (Martinez-Mera, 2007). By adding ferric and ferrous chloride in the presence of a base magnetite will precipitate. The silica magnetite composites were created by co-precipitation. The following chemical equation represents the reaction that takes place for the precipitation of magnetite (Martinez-Mera, 2007) and the following table shows the properties of the particles used in this research.

$$2Fe^{3+} + Fe^{2+} + 4OH^- \rightarrow Fe_3O_4 + 4H_2O$$

Table 3. Properties of particles.

Name	Specific Surface Area (g/m^2)	Silica to Magnetite Ratio
Commecial Magnetite	88	N/A
Dispersed Commercial Magnetite	88	N/A
Silica Coated Commercial Magnetite	52.9	3.48 to 1
Magnetite Silica Composite	489	4 to 1
Hydrogen Reduced Magnetite Silica Composite	479	4 to 1

A Frantz Ferrofilter, purchased from S.G. Frantz Company Incorporation, model PRE-1 was used for filtrations. The main components of the filter are two permanent magnets, a

column, and a stainless steel mesh. According to the manufacture the permanent magnets induce a field of 4,800 Gauss or 0.48 Tesla within the column. The cross-sectional area of the column is 10.12 cm^2 and the stainless steel mesh is 14 cm long. Two openings allow for the attachment of tubing. The following pictures are of the filter and the stainless steel mesh.

Figure 22. Frantz ferror filter.

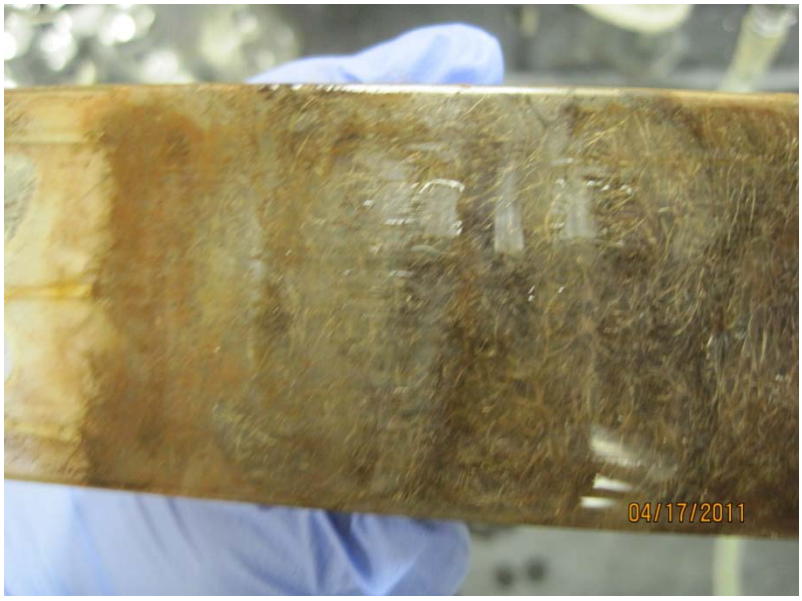

Figure 23. Stainless steel mesh.

Two different pumps were used: a FMI Lab Pump model QV from CERAMPUMP and an Eastern Industries pump model E-7. The FMI pump flowrate was controlled with an FMI stroke rate controller model V200. The Eastern Industries pump was controlled with a Variac controller type W5MT3. A Cole-Parmer Instruments Universal Motor with a propeller attached was used as a mixer to disperse the solution and was also controlled by a Variac controller type W5M.

An additional gravity fed column was constructed. This setup used the magnets provided by S.G. Frantz Company and consisted of a packed funnel packed with Grade 3 steel wool from Grainger International Inc. The packing fraction of the gravity fed filter was 0.68 grams of stainless steel wool per ml of volume. The stainless steel wool was replaced between filtrations. A picture of this column during a filtration can be seen below.

Figure 24. Gravity fed funnel column.

A demagnetizer was fabricated from a motor. Objects can be demagnetized by oscillating a magnetic field through the substance and decreasing the amplitude of the oscillations. This was accomplished by removing the shaft out of a motor. The amplitude of the oscillations was controlled by varying the power into the motor with a Variac controller type W5MT3. A picture of the demagnetizer can be seen below.

Figure 25. Demagnetizer.

Experimental methods

Two different slurry concentrations were used 250 mg/L and 500 mg/L. When completing a dispersed filtration, sodium polyphosphate was added at a concentration of 10% of the concentration of magnetite particles. Magnetite was dispersed in solution by sonication. A QSonica Mizonix Ultrasonic Liquid Processor model S-4000 was used for sonication. Slurries were allowed to cool after sonication. The following table and figures show the parameters used during sonication and the slurry before, during, and after sonication.

Table 4. Parameters used during sonication.

Parameter	Value	
Time:	25	minutes
Amplitude:	15	μm
Position (from bottom):	0.5	inch

Probe Size: 1 inch

Figure 26. Magnetite in solution before, during, and after sonication from left to right.

After the slurry was prepared the mixtures were stirred and pumped at a constant flowrate through the Ferrofilter with the provided column. Samples were taken at regular time intervals and pipetted to a volume of 1 ml. In the case of the gravity fed filter the slurries were allowed to flow through the filter and samples were taken from the effluent and averaged after the filtration was completed. The magnetite samples were then dissolved with hydrochloric acid or a combination of hydrochloric and nitric acid; nitric acid was used because it creates a more preferable matrix for analysis with atomic absorption (Greenberg 1992). Upon dissolution, the solutions could be analyzed for total iron and the magnetite concentration could be calculated using the stoichiometry of the dissolution reaction. Two methods were used to analyze samples colorimetric and atomic adsorption; these methods will be discussed in more detail later.

The filter was then backwashed at an elevated flowrate to remove collected particles from the stainless steel matrix. It was found that the magnetite particles would not efficiently be removed from the filter media with distilled water alone. By elevating the pH of the water to about 10.8 by making a 10^{-3} M sodium hydroxide solution as completed by Svoboda (1985) recovery became much more effective. The backwash of particles dispersed with sodium polyphosphate was completed efficiency with distilled water alone. The column was also demagnetized during a backwash to achieve even higher recovery.

A filtration in series was also completed by filtering the magnetite slurry, backwashing the filter, and refiltering the filtrate. This was completed to see if it enhanced the capture efficiency of the slurries by subjecting them to a longer residence time in the filter. Samples were taken at regular intervals to determine the capture efficiency of the filter. The diagram below represents the filter in series.

Figure 27. Representation of a filtration in series.

The Phenanthroline Method of analysis (Greenberg 1992) was used to determine the total iron content by spectrophotometry. Iron standards were mixed to concentrations of 0.5, 1, 1.5, 2.0, and 2.5 mg/L. A FerroVer Iron Reagent pillow was then added to buffer the solution and create the color. Since the colored solutions obey Beer's law, a linear relationship between absorbance and concentration occurs. Samples were diluted within the range of the standards and the FerroVer Iron Reagent pillows were added to the samples. The absorbance of the standards were then measured followed by the absorbance of the samples. The sample concentrations were interpolated from the standard assay curve by the software automatically. The spectrophotometer used was a Varian Cary 50 Bio. The parameters used during spectrophotometry are listed below.

Table 5. Parameters used during spectrophotometry.

Parameter	Value
Instrument:	Cary 50
Instrument Version No.:	1
Wavelength (nm):	510
Ordinate Mode:	Abs
Ave Time (sec):	0.1
Replicates 2:	2
Stadnard/Sample Averaging:	OFF
Weight and Volume Corrections:	OFF
Fit Type:	Linear Direct
Min R^2:	0.95
Concentration Units:	mg/L

Atomic absorption was also used to analysis samples for total iron content. A bulk stock solution of 60 ppb iron was created. The atomic absorber then atomizes different volumes of the stock solution to create a standard curve of absorbance versus concentration. In this case, the absorbance of a standard or sample is related to the total amount of the ions being atomized, not the concentration of the solution. By changing the volume of standard solution used the absorbance would change. The absorbance emitted from the atomization of 5 μL, 10 μL, and 15 μL of standard would correspond to 30, 60, and 90 ppb iron concentrations, respectively. Makeup water was added to each standard volume so that the total volume injected remained constant, but the volume from the bulk would change. Subsequently, the samples were atomized and their concentrations were interpolated from a nonlinear curve created by the machine's software. A Varian 240 atomic absorber with a Zeeman furnace was used. The following two tables show the furnace operating conditions and instrument parameters used.

Table 6. Operating conditions used for analysis.

Step No	Temp deg C	Time sec	Gas Flow L/min	Gas Type	Read	Store
1	85	5	0.3	Normal	No	No
2	95	40	0.3	Normal	No	No
3	120	10	0.3	Normal	No	No
4	700	5	0.3	Normal	No	No
5	700	1	0.3	Normal	No	No
6	700	2	0	Normal	No	Yes
7	2300	0.8	0	Normal	Yes	Yes
8	2300	2	0	Normal	Yes	Yes
9	2300	2	0.3	Normal	No	Yes

Table 7. Instrument parameters used for analysis.

Parameter	Value	
Lamp Current:	8	mA
Spectral Bandwidth:	0.2	nm
Wavelength:	248.3	nm
Maximum Absorbance:	0.9	
MSR%:	97%	

Sample calculations

The following chemical equation represents the dissolution of magnetite in solution and the calculation used to determine the magnetite concentration from the total iron concentration obtained during analysis where [*Magnetite*] and [*Fe*] in mg/L are the concentrations of magnetite and iron and DF is a factor to account for dilution.

$$Fe_3O_4 + 8H^+ \rightarrow 2Fe^{3+} + Fe^{2+} + 4H_2O$$

$$[Magnetite] = [Fe]\frac{231.54}{55.84 * 3} * DF$$

Once the concentration of magnetite was calculated, the percent passing and captured efficiency could be calculated with the following equations where $[Magnetite]_S$ and $[Magnetite]_0$ are the concentration of magnetite in the sample and the initial concentration of magnetite.

$$\%Pas\sin g = \frac{[Magnetite]_S}{[Magnetite]_0} * 100$$

$$\%Capture = 1 - \%Pas\sin g$$

The mass of particles captured M_{cap} and the mass of particles recovered M_{rec} from subsequent backwashes were also calculated by using a trapezoidal approximation method. This averages the concentration of particles over a given time interval *n* and multiplies by the volume of fluid passing through the filter over that given time interval. This equation is as follows where *Q* is the flowrate and *t* is time. The subscript represents the interval at which the sample was taken, whether from the filtrate or the backwash.

$$M_{cap} = M_{rec} = \frac{[Magnetite]_{S(n)} + [Magnetite]_{S(n+1)}}{2} * Q(t_{n+1} - t_n)$$

Chapter 4

Results and Discussion

First, a comparison of capture efficiency to flowrate is presented for magnetite and magnetite dispersed with sodium tripolyphosphate. Then, the results for the capture of slurries with different particle concentrations are shown, again for both magnetite and dispersed magnetite. After that, the capture efficiency for magnetite, dispersed magnetite, and magnetite coated with silica are given. Next, the result from the filtration in series is displayed followed by the gravity fed filtration's results. Finally, the particle recovery data is presented. It was found that as flowrate increased, the particle capture decreased due to increased viscous forces. As particle loading increased, the capture efficiency decreased due to diffusion limitations. Magnetite was more efficiently removed compared to magnetite dispersed with sodium tripolyphosphate and magnetite coated with silica because the solution was less stable. The gravity fed funnel filter provided the highest capture efficiencies.

Effect of flowrate on capture efficiency of magnetite nanoparticles

The filtration of 500 mg/L magnetite slurries were completed at three different velocities through the cross-section: 1, 2.7, and 4 cm/s. The average capture efficiency for the 1, 2.7, and 4 cm/s filtrations were 98.6%, 96.9%, and 92.5% respectively. These results are expected since an increase in velocity will increase the viscous force exerted on the particles, which opposes the magnetic force. Also, a decrease in the residence time occurs so the particles are less likely to adhere to the column. The following table and figure shows the change in capture efficiency over time for the different flow rates. Particle concentrations were taken at different time intervals due to limitations with total volumes of slurries.

Table 8. Capture Efficiency of 500 mg/L Magnetite Slurries.

Time, sec	Velocity, cm/s 1	2.7	4
10		96.0%	95.5%
20	98.0%	96.1%	92.3%
30		96.8%	91.4%
40	98.5%	96.7%	91.3%
50		97.1%	
60	100.0%	98.1%	
70		97.2%	
80	98.5%		
100	98.6%		
120	98.0%		
140	98.6%		
160	98.6%		

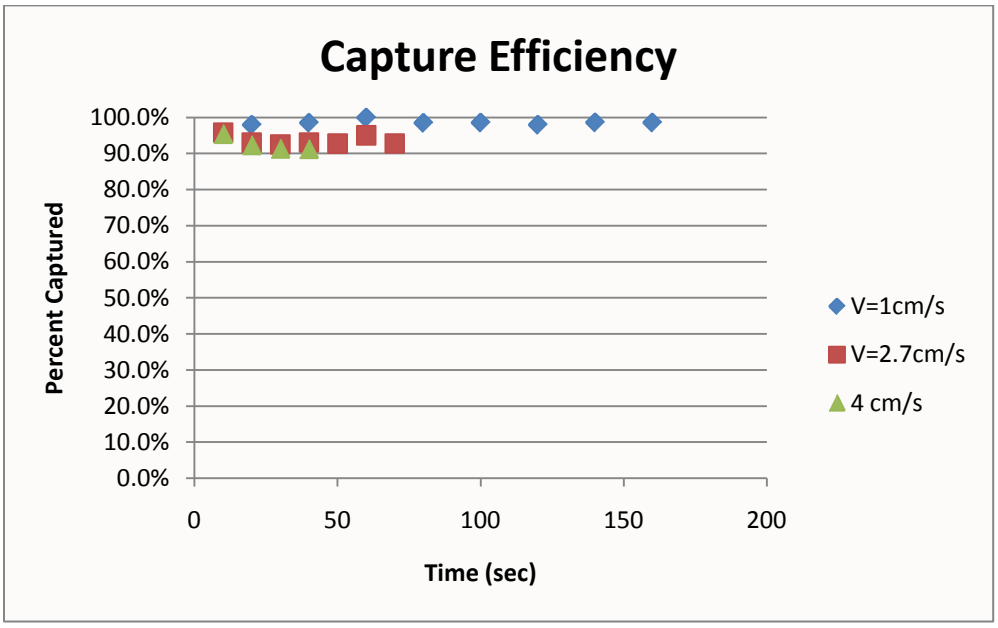

Figure 28. Capture efficiency of 500 mg/l magnetite solutions.

Effect of flowrate on dispersed magnetite capture efficiency

The results for the filtration of 500 mg/L magnetite slurry at velocities of 0.6, 0.8, and 1 cm/sec are presented in this section. The average capture efficiencies for the 0.6, 0.8, and 1 cm/sec filtration were found to be 76.0%, 60.8%, and 43.5%, respectively. Again the increase in flowrate decreased the capture efficiency of the particles due to increased shear forces and decreased residence time. The results from these filtrations were much more variable due the lower capture efficiency and greater stability of the particles. A summary of the results can be seen in the following table and figure.

Table 9. Capture Efficiency of Magnetite Dispersed with Sodium Tripolyphosphate.

Time,	Velocity, cm/s		
sec	0.6	0.8	1
20		64.3%	41.9%
30	80.1%		
40		62.7%	52.8%
60	74.9%	61.3%	39.8%
80		63.9%	47.7%
90	76.0%		
100		63.6%	41.2%
120	76.3%	64.6%	39.4%
140		65.0%	48.2%
150	79.8%		
160		63.6%	36.9%
180	77.8%	64.7%	
200		39.2%	
210	74.3%		
220		55.9%	
230	68.8%		

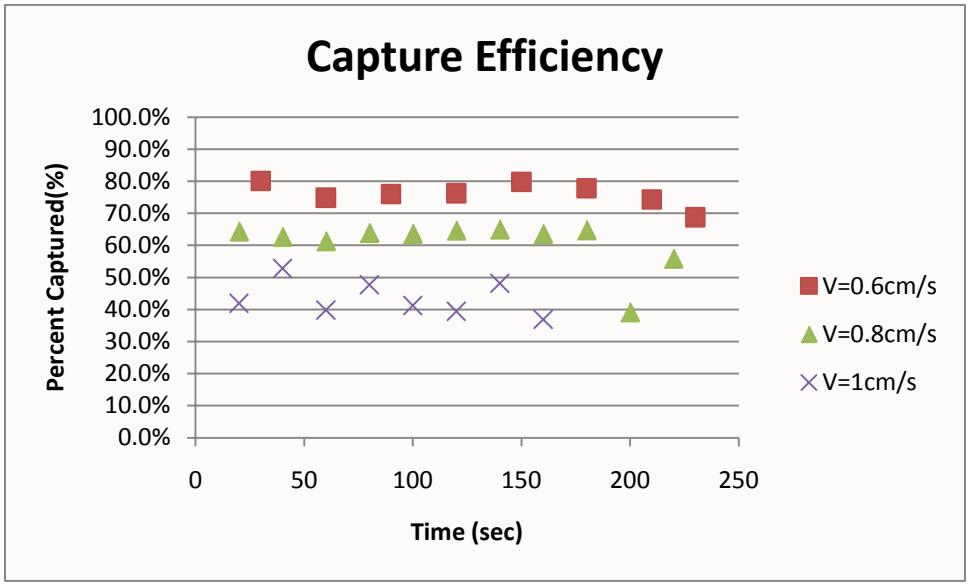

Figure 29. Capture efficiency of magnetite dispersed with tripolyphosphate.

Particle loading comparison for magnetite

Two different concentrations of magnetite, 250 and 500 mg/L, were filtered at a constant velocity of 2.7 cm/sec. It was found that the average capture efficiency for particle loadings of 250 and 500 mg/L were 96.9% and 93.6%, respectively. It was expected that an increase in particle loading would increase the capture efficiency of the filter since the mixture would be less stable causing the particles to aggregate more rapidly. This can be better explained by the following equation for the rate of buildup where n_o is the number density of particles far from the wire, C represents the quantity of particles that have built up already, n_s is the number density of particles in the buildup region, L is the height of the theoretical plate, and V_o is the open tube velocity (Ditsch 2005).

$$\frac{\partial B}{\partial t} = \frac{n_o C}{n_s L} V_o$$

For this scenario, all of the variables can be considered near constant for each particle loading except for n_o. This indicates that when the particle loading doubles the rate at which build up occur should double, which is nearly the case for this situation. This is nearly true in this case since 93% of 500mg/L is approximately twice 96.9% of 250 mg/L. The decrease in the rate at which the particles buildup can be attributed to diffusion; as more particles try to attach to the wire at a given position the less likely they are to attach. The following table and figure compare the capture efficiencies for various particle loadings of magnetite.

Table 10. Capture efficiency of magnetite at a velocity of 2.7 cm/sec with varying particle loadings.

Time, sec	Particle Loading, mg/L 250	500
10	96.0%	95.81%
20	96.1%	93.01%
30	96.8%	92.54%
40	96.7%	93.06%
50	97.1%	92.75%
60	98.1%	95.06%
70	97.2%	92.79%

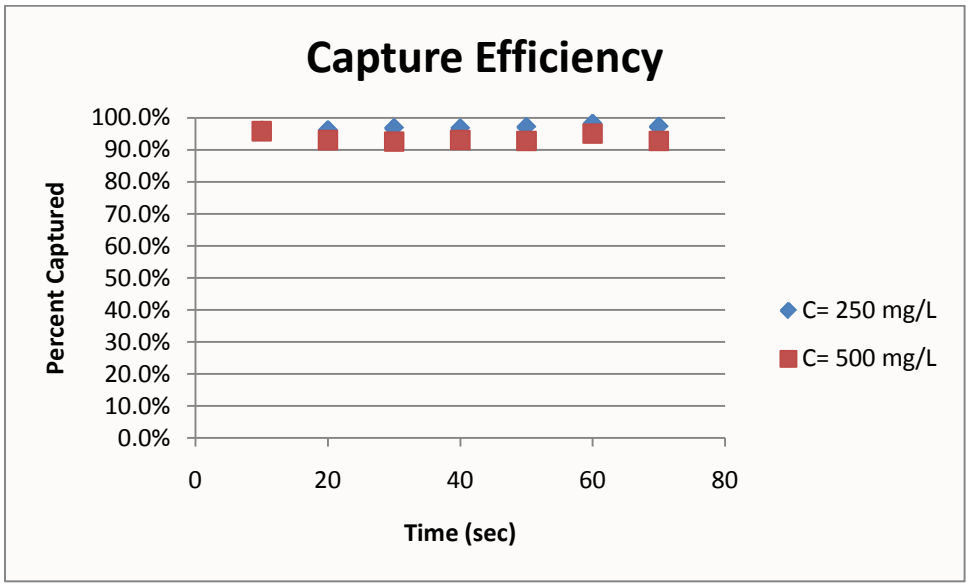

Figure 30. Capture efficiency of magnetite at a velocity of 2.7 cm/sec with varying particle loadings.

Particle loading comparison for dispersed magnetite

Two different magnetite slurries containing particle loadings of 250 mg/L and 500 mg/L magnetite and 25 mg/L and 50 mg/L sodium tripolyphosphate as a dispersant, respectively, were filtered at a constant approach velocity of 0.6 cm/sec. It was found that the average capture efficiency for the 250 mg/L and 500 mg/L slurries were 90.3% and 76.9%, respectively. This can be explained by the rate at which particles buildup. In this case, capture efficiency of the higher concentrated slurry dropped more significantly. This is due to the interactive forces between the particles. The dispersant causes the particles to repel each other by increasing the electric double layer. So, when the particles become more confined and move towards the wire they move more sporadically, decreasing the chances of their capture compared to the case where the particles have more favorable surface interactions. The following table and figure show these results.

Table 11. Dispersed separation comparison of particle loadings of 250 mg/L and 500 mg/L at 0.6 cm/sec.

Time, sec	Particle Loading, mg/L 250	500
10	93.9%	83.8%
20	92.5%	79.3%
30	89.8%	79.5%
40	88.9%	75.4%
50	89.5%	75.8%
60	88.9%	68.6%
70	88.9%	76.5%
80	89.5%	76.2%

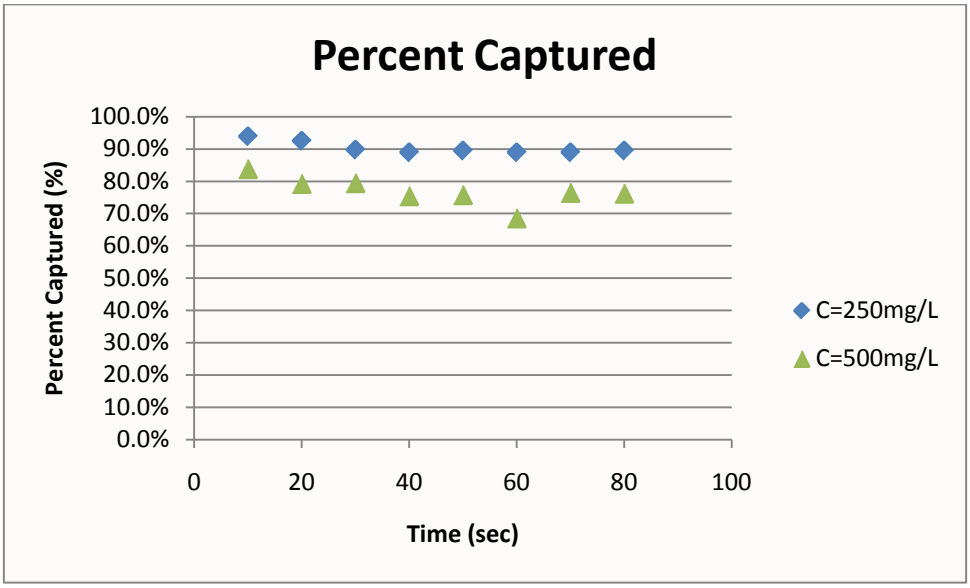

Figure 31. Dispersed separation comparison of particle loadings of 250 mg/L and 500 mg/L at 0.6 cm/sec.

Comparison of filtrations efficiencies for nondispersed, dispersed, and silica coated magnetite

Three different slurries containing 500 mg/L of magnetite, magnetite dispersed with sodium tripolyphosphate, and magnetite coated with silica were created and pumped through the filter at a constant velocity through the cross section of 1.0 cm/sec. The average capture efficiency for the magnetite, dispersed magnetite, and silica coated magnetite were 98.6%, 43.5%, and 75.1%, respectively. These results indicate that magnetite is the least stable in solution, followed by the silica coated magnetite and the dispersed magnetite. This also indicates that the stability of the particles in solution plays a large role in the capture of particles in water. Viscous effects are more significant on the silica coated particles, since they are larger, but the core of the particle is a commercial magnetite particle so the imposed magnetic moment on the particle is relatively close to that of a magnetite particle. Additionally, silica coated particles are more stable in water which probably plays a larger role in their capture compared to the viscous force, since all of the particles are relatively small. The significances of the stability of the particles are further demonstrated by the dispersed particles. Since the same particles are being used, the hydrophilic conditions imposed on the particles by the dispersant account for the loss in capture efficiency. This indicates that the dispersed magnetite is more stable than the silica coated magnetite. The following table and figure show the temporal particle capture efficiencies. The filtration for the silica coated commercial magnetite was shorter because a small quantity of particles was provided.

Table 12. Non-dispersed, dispersed, and silica coated particle capture efficiency over time.

Time,	Particle Type		
sec	Non-Dispersed	Dispersed	Silica Coated
20	98.0%	41.9%	75.3%
40	98.5%	52.8%	76.0%
60	100.0%	39.8%	74.2%
80	98.5%	47.7%	75.8%
100	98.6%	41.2%	74.1%
120	98.0%	39.4%	
140	98.6%	48.2%	
160	98.6%	36.9%	

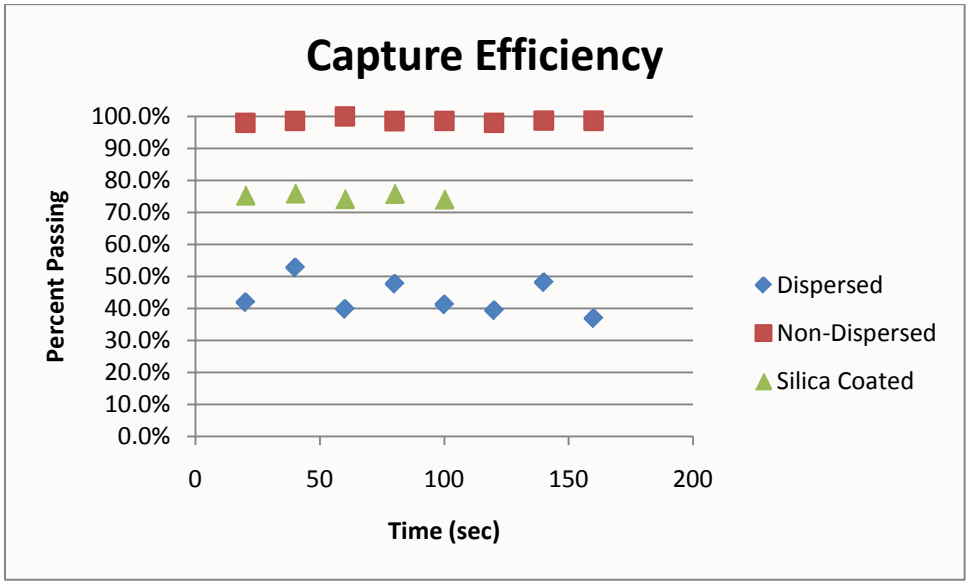

Figure 32. Non-Dispersed, Dispersed, and Silica coated magnetite capture efficiency over time.

Filtration in series

Due to the relatively low capture efficiency of dispersed magnetite, one filtration in series was completed in order to determine if a further capture of particles could be achieved. A 500 mg/L magnetite slurry was created and pumped through the filter twice at a constant velocity of 0.6 cm/s. Filtering the particles twice simulates a residence time twice that of the initial residence time. The average concentration of particles exiting the separator for cycles 1 and 2, relative to the initial concentration of particles, was 76.0% and 89.5%, respectively. This indicates that more particles can be captured with a longer residence time, and the particles filtered in the second cycle are smaller particles. The concentration of the particles leaving the filter after the first cycle was about 120 mg/L. The decrease in the concentration of the particles leaving the filter after the second cycle is less, with a final concentration of about 52.5 mg/L. The overall capture efficiency decreased from 76.0% to 56.3%. Since a lower particle concentration achieved higher capture efficiency previously, this is either due to a decrease in the particle size or incomplete knowledge of the effects of the change of concentration on capture efficiency. The temporal change in particle concentration for each cycle can be viewed in the table and figure below.

Table 13. The change in the capture efficiency of dispersed magnetite for multiple cycle filtrations.

Time, sec	Cycle Number 1	2
30	80.1%	89.6%
60	74.9%	91.1%
90	76.0%	90.3%
120	76.3%	85.9%
150	79.8%	90.3%
180	77.8%	89.6%
210	74.3%	89.6%
227	68.8%	

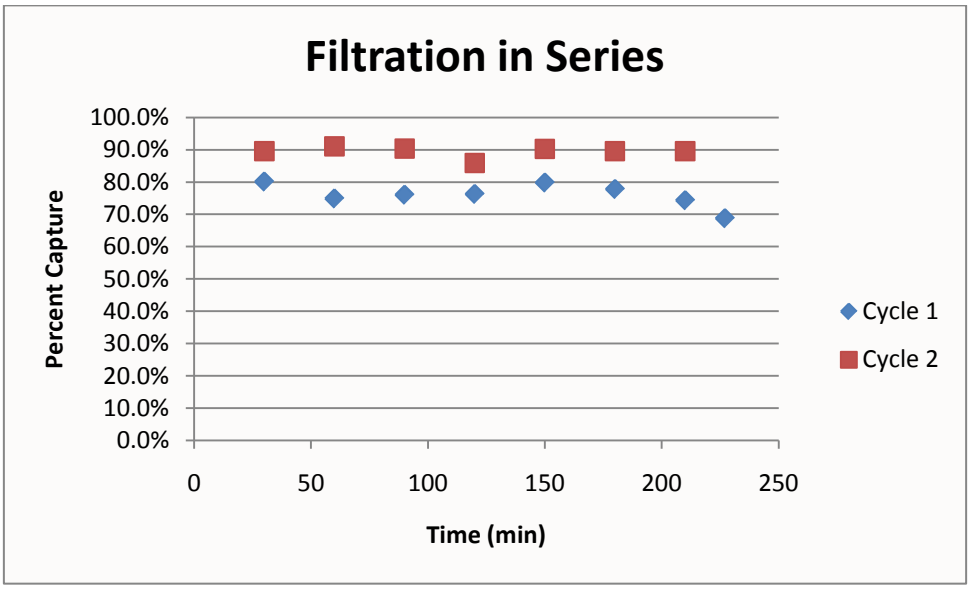

Figure 33. The change in the capture efficiency of dispersed magnetite for multiple cycle filtrations.

Gravity fed funnel column

A gravity fed HGMS was also developed and the commercial magnetite (1), the silica coated commercial magnetite (2), the dispersed commercial magnetite (3), and a magnetite silica composite before (4) and after (5) hydrogen reduction were filtered through the HGMS. The silica to magnetite mole ratio for the silica coated commercial magnetite and the silica magnetite composites were 3.48 and 4, respectively. The stainless steel wool was replaced after each filtration and the filter was cleaned. The average velocity through the filter was 3.6, 3.9, 4.2, 3.7, and 3.5 for samples 1 through 5, respectively. The variations in velocity were due to the hydraulics through the filter. The highest capture efficiency was achieved for the commercial magnetite at 99.8%. The hydrogen reduced silica magnetite composite had the next highest capture efficiency at 97.9%, followed by silica coated commercial magnetite at 96.7%. The silica magnetite composite without hydrogen reduction was captured at 95.0%, and the dispersed magnetite at 78.6%. For the commercial magnetite and commercial magnetite silica composites, the net magnetic strength on a given particle can be expected to be nearly the same since the core of the silica coated magnetite particle is a commercial magnetite particle. This indicates that the drop in the capture efficiency is due to an increase in the stability of the particle and the viscous force imposed on the particle. By direct observation of the particles around magnets, it seems that the commercial magnetite has a larger magnetic strength than both the magnetite silica composites. Additionally, hydrogen reduction increases the magnetic strength which explains an increase in capture efficiency for these particles. This also shows that the more stable dispersed magnetite is still significantly less separable. The results from these filtrations are summarized in the following table.

Table 14. Percent removal from the gravity fed filter.

Sample Comparison - Percent Removal				
1	2	3	4	5
Commercial Magnetite	SiO_2/Mag 3.48/1	Dispersed Magnetite	SiO_2/Mag 4/1	SiO_2/Mag (H.R.) 4/1
99.8%	96.7%	78.6%	95.0%	97.9%

Particle recovery

Magnetite

The recovery of non-dispersed magnetite particles in magnetic filters is strongly dependent on the pH of the backwash fluid (Svoboda 1985). A 500 mg/L magnetite solution was made and pumped through the filter at a constant velocity of 1 cm/sec. The filter was then backwashed with water of a pH of 10.8 at a velocity of 1 cm/sec. The total mass captured was found to be approximately 360 mg and the total mass recovered was found to be 110 mg. Incomplete capture of the particles is most likely due to insignificant backwash flowrate. Additionally, a longer backwash would have removed more particles since the mass of particles recovered had not completely tapered off yet. Some residual magnetism in the filter's mesh causes the particles to remain on the filter. A higher backwash velocity can overcome this problem to some extent. The following figures are of the cumulative mass captured and recovered.

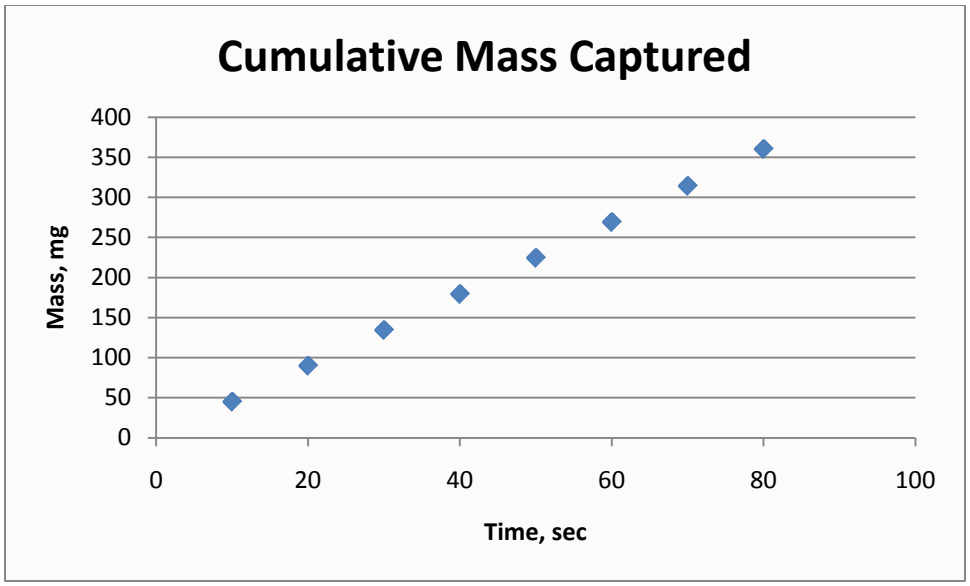

Figure 34. Cumulative mass captured from a 1 cm/s 500 mg/L filtration.

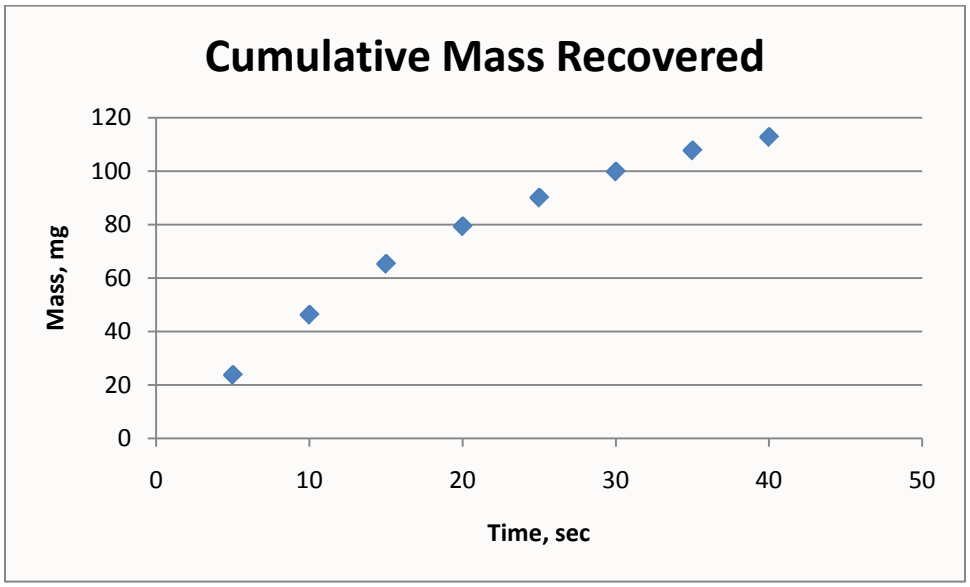

Figure 35. Cumulative Mass Recovered of 1 cm/s and pH of 10.8.

A magnetite slurry of 500 mg/L was filtered at a velocity of 2.7 cm/sec to obtain the cumulative mass over time. The filter was then backwashed at a velocity of 6.7 cm/sec and two samples were taken from the backwash fluid. The cumulative mass captured was approximately 890 mg, and the cumulative mass recovered was approximately 1220 mg. Possible reasons for this discrepancy are that particles from previous filtrations were dislodged during the backwash or inaccuracies in the approximation method. The concentration of particles leaving the filter after 5 seconds was very high at 2,380 mg/L and dropped rapidly to 122 mg/L at the 10 second interval. This is due to the large backwash velocity and may be subjected to serious error when averaging the particle concentration between time intervals. Although a mass balance was not achieved this indicates that a majority of the particles can be removed from the filter. The following two figures show the cumulative mass captured and the cumulative mass recovered.

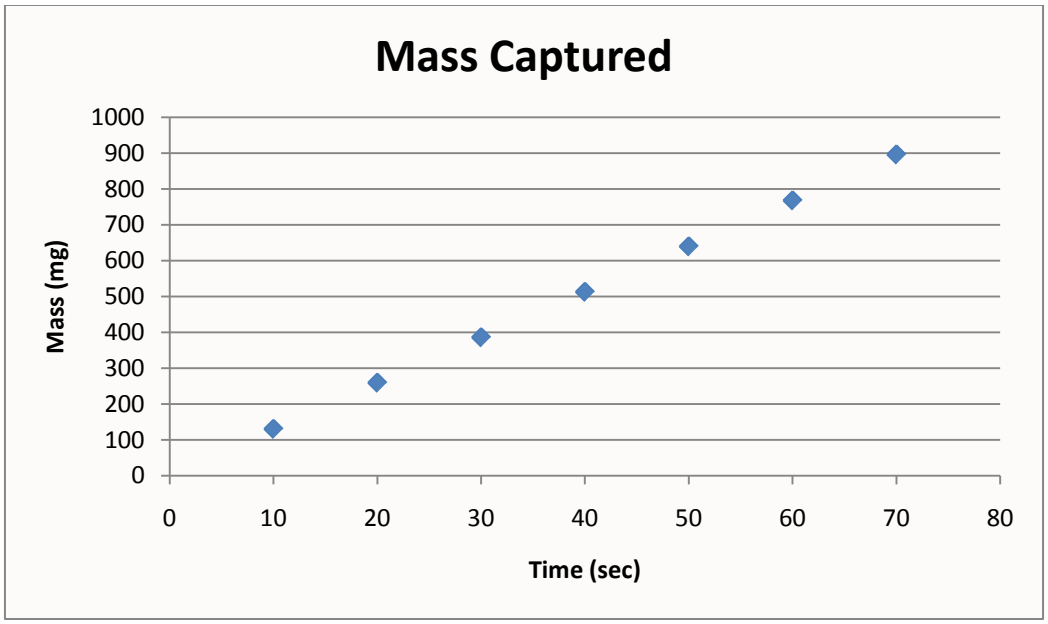

Figure 36. Cumulative mass captured from a 2.7 cm/s 500 mg/L filtration.

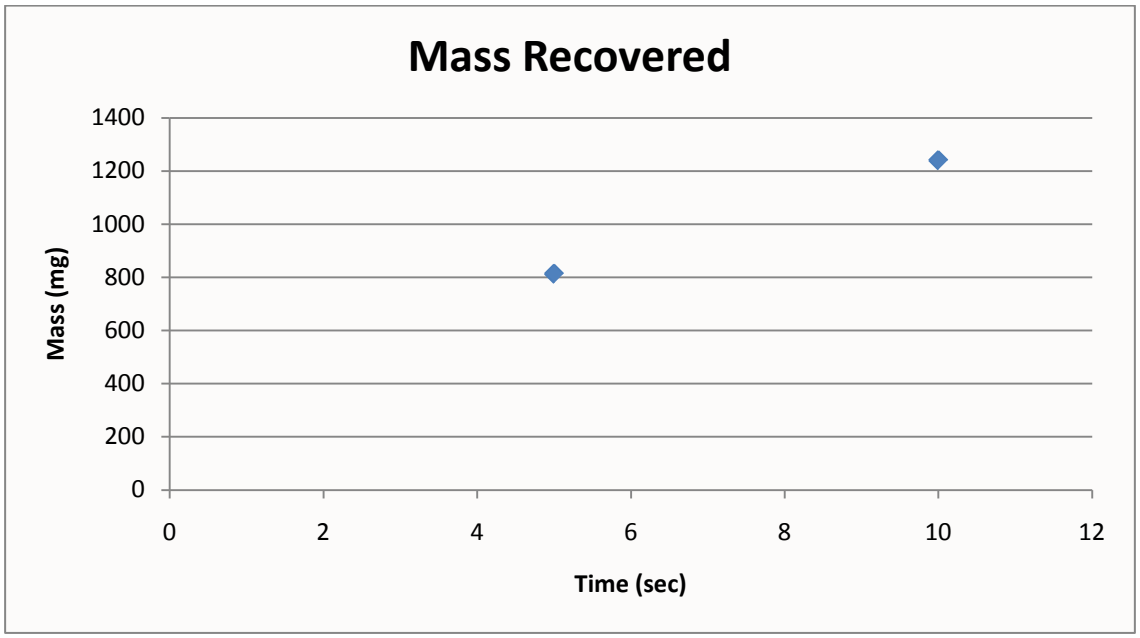

Figure 37. Cumulative mass recovered at a velocity of 6.7 cm/s and pH of 10.8.

A backwash through a gravity fed filter was completed. A 1 L magnetite slurry was created and filtered with an average velocity of 3.6 cm/s. The filter was then demagnetized. The backwash water had a pH of 10.9 and the filter was flushed at a velocity of 22.1 cm/s. The percent of particles captured and recovered were 99.8% and 88.8%, respectively where the percent recovered was the mass captured divided by the mass recovered. A total of 0.557 L of water was used to recover the particles. The backwash solution then became dilute and it was no longer efficient to continue the process. Magnetite particles are recoverable by increasing the pH to create preferable surface conditions and removing residual magnetism from the column. The following table summarizes the results.

Table 15. Mass of particles captured and recovered for a gravity fed filtration.

Percent Captured	Percent Recovered
99.8%	88.8%

Dispersed Magnetite

Dispersed magnetite particles are more easily recovered than magnetite particles alone. The pH of the solution does not need to be adjusted and the particles can be recovered at lower velocities. A filtration run was conducted with a particle loading of 250 mg/L and velocity of 0.6 cm/sec. The total mass captured was approximately 105 mg. The filter was then backwashed at a rate of 0.7 cm/sec. The cumulative mass recovered was about 41 mg, which is substantially less than the total mass accumulated. The particle concentration in the effluent was not leveling off and incomplete recovery can be attributed to insufficient backwash velocities and too short of backwash time. It does indicate that the particles can be removed from the filter at a relatively low velocity. The following two figures represent the cumulative mass captured and recovered.

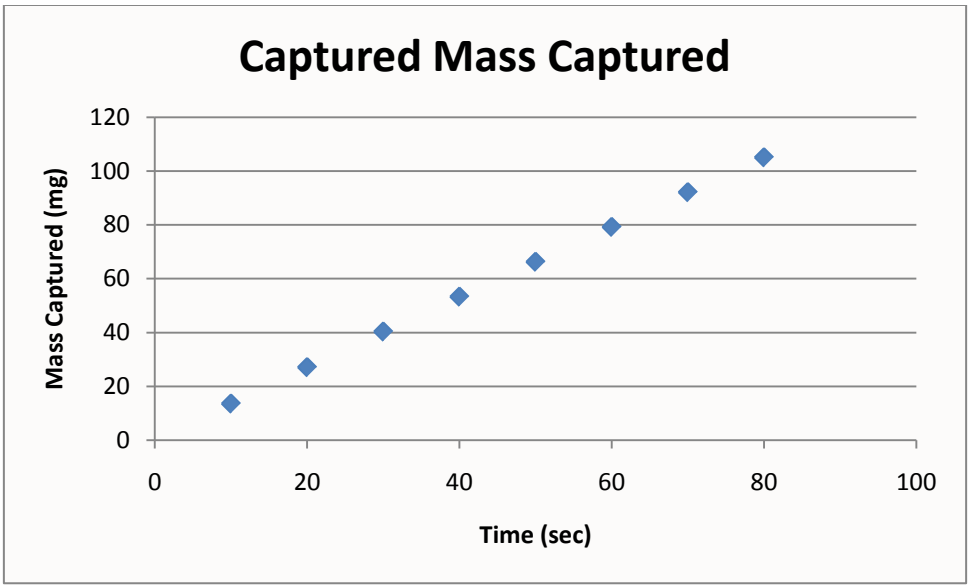

Figure 38. Cumulative mass captured from a 0.6 cm/s, 250 mg/L filtration.

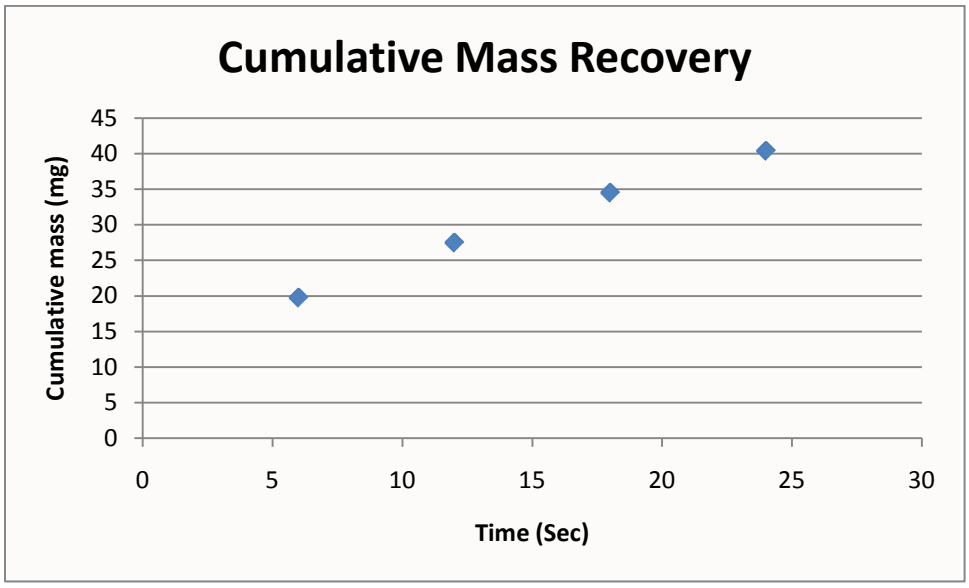

Figure 39. Cumulative mass recovered at a velocity of 0.7 cm/sec.

The next backwash was completed for a 0.6 cm/sec filtration with a particle loading of 500 mg/L. In this case, the total mass of particles captured was about 750 mg. The filter was backwashed at 0.8 cm/sec to recover the particles. The total mass of particles recovered was approximately 375 mg. This recovery is less than the total quantity of particles retained on the filter due the low velocity. Since the curve levels off, it also shows that the backwash time was not the limiting factor. The following two figures show the cumulative mass captured and the cumulative mass recovered.

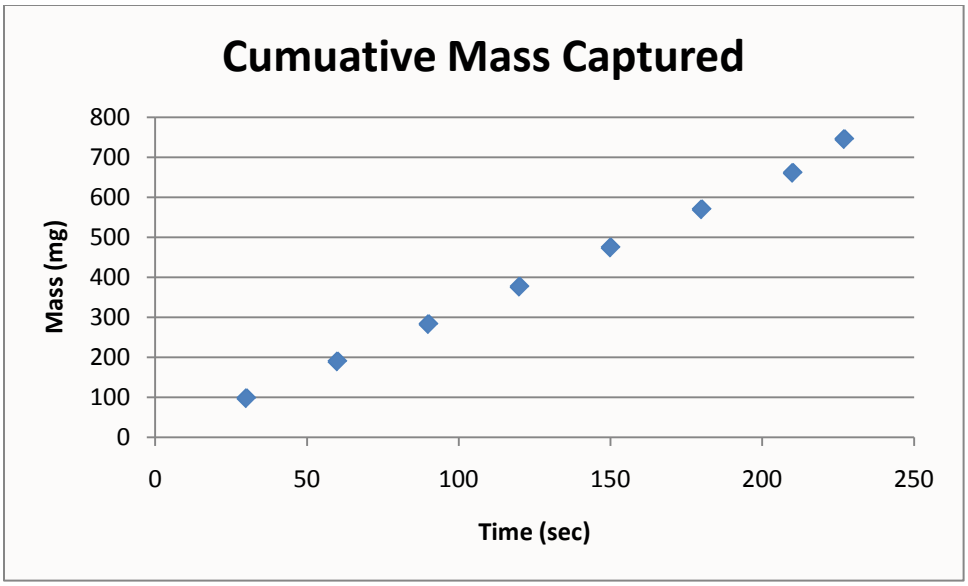

Figure 40. Cumulative mass captured from a 0.6 cm/sec, 500 mg/L filtration.

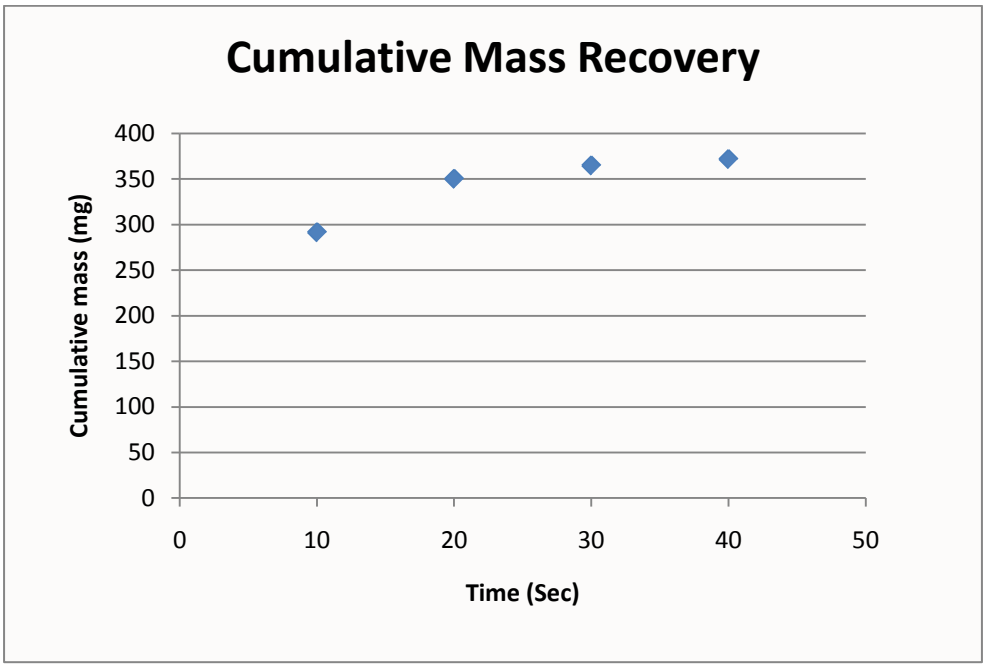

Figure 41. Cumulative mass recovered at a velocity of 0.8 cm/sec.

Another filtration was completed at 0.8 cm/sec with a particle loading of 500 mg/L. The cumulative mass captured was about 550 mg. A backwash was completed at 1 cm/sec to recover the particles. The cumulative amount of particles recovered was 650 mg, which is slightly higher than the amount of particles captured. The error may be due to the inaccuracy of the approximation method or from residual particles that were expelled in the backwash. The mass of the particles recovered levels off rapidly after 20 seconds indicating that a sufficiently long backwash was completed, and the mass of particles recovered shows that a sufficient velocity was used. The following two figures represent the cumulative mass captured and recovered.

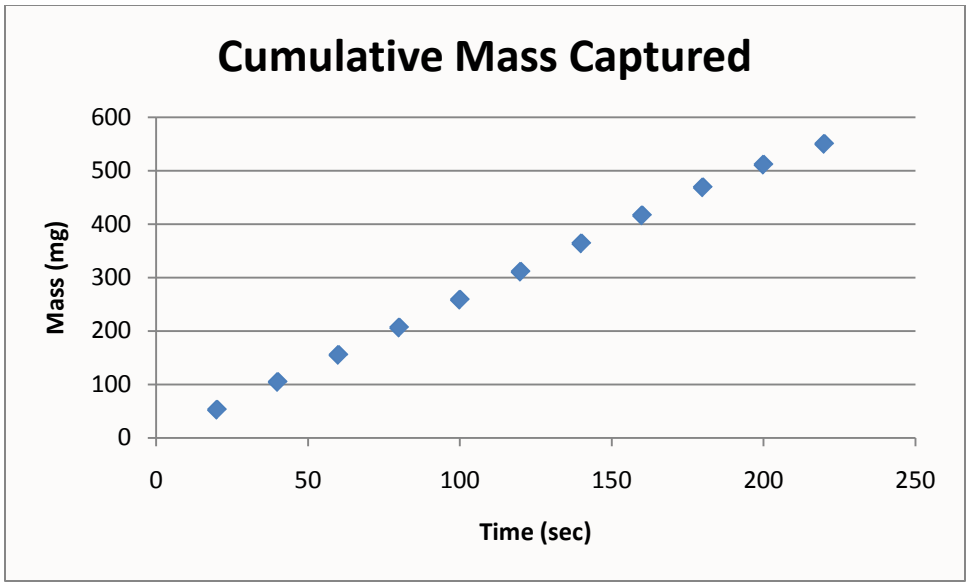

Figure 42. Cumulative mass capture at 0.8 cm/sec and 500 mg/L.

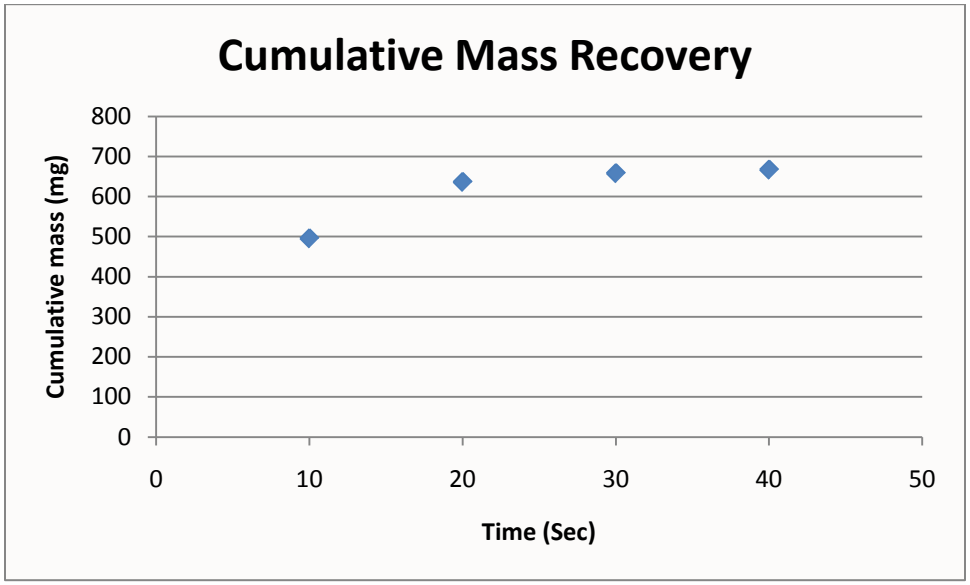

Figure 43. Cumulative mass recovered at a velocity of 1 cm/sec.

Chapter 5

Conclusions and Recommendations

Conclusions and Summary

1. The effect of the velocity of the filtration on capture efficiency was examined through the Frantz Ferro Filter. It was found that as the velocity increased, the particle capture efficiency decreased due to an increase in viscous forces on the particle. The effect of particle velocity was significantly less for magnetite alone. The particle capture efficiency remained greater than 90% for velocities ranging from 1 cm/s to 4 cm/s for magnetite. These velocities seem low, but given the length of column, 14 cm, the residence times are sufficiently low ranging from 14 to 3.5 seconds. Additionally, at a velocity of 1 cm/s, the average capture efficiency was 98.6% which is substantial for the given magnetic flux. The flow velocity significantly affected the capture efficiency of magnetite dispersed with sodium tripolyphophate. The average capture efficiency dropped from 76% at 0.6 cm/s to 43.5% at 1 cm/s. The commercial magnetite was coated with silica and filtered at 1 cm/s. An average capture efficiency of 75.1% was achieved for the silica coated magnetite particles. The net magnetism on a given particle is about the same as the commercial magnetite particle since the core of the particle is a commercial magnetite particle, which is modeled as such in Moeser's *High-Gradient Magnetic Separation of Coated Magnetic Nanoparticles*. Therefore, the decrease in capture efficiency is due to an increase in the stability of the particles; this also indicates that the stability of the dispersed particles is greater than the commercial magnetite coated with silica. The total viscous force on the commercial magnetite coated with silica is probably greater because they are larger. This may also play a role in their decrease in capture efficiency compared to the magnetite particles.

2. The particle loading was also adjusted in order to determine if this affected the capture efficiency. It was found that lower particle loadings had greater capture efficiency for both the dispersed and non-dispersed magnetite particle. This is most likely due to the effects of diffusion; the greater the number of particles trying to attach to a given spot on the wire, the less likely they can all diffusion onto the wire. For non-dispersed particles, the effects of particle loading were less significant only dropping from 96.9% capture for 250 mg/L to 93.6% capture for 500 mg/L. For dispersed magnetite, the capture efficiency dropped from 90.3% to 76.9%.

The difference is likely due to the stability of the particles; there are significantly more repulsive forces in the dispersed system, and this makes diffusion more difficult. The non-dispersed magnetite may have even formed aggregates.

3. Two-stage filtration in series was completed in order to determine if a longer residence time would affect the capture efficiency of dispersed magnetite particles. It was found that the average capture efficiency for cycle 1 was approximately 76.0% and the average capture efficiency for cycle 2 was 89.5% of the initial concentration. This indicates that a larger retention time would increase the capture efficiency but there are most likely still some limitations on the total capture efficiency, since a large amount of the total capture efficiency was completed in cycle 1.

4. A gravity fed HGMS was also developed by putting stainless steel wool inside of a column. Several different particle slurries were filtered using this setup including commercial magnetite, dispersed commercial magnetite, commercial magnetite coated with silica, and magnetite silica composite with and without hydrogen reduction. The commercial magnetite had the greatest capture efficiency at 99.8% at 3.6 cm/s. The dispersed commercial magnetite was captured at an efficiency of 78.6% for a velocity of 4.2 cm/s. The commercial magnetite coated with silica was captured at an efficiency of 96.7% for a velocity of 3.9 cm/s. The synthesized magnetite silica composite was capture at an efficiency of 95.0% before hydrogen reduction at 3.7 cm/s and at 97.9% after hydrogen reduction for a velocity of 3.5 cm/s. The commercial magnetite achieved the highest capture efficiency since it is the least stable, most magnetic particle. The silica coated commercial magnetite has similar magnetic strength to the commercial magnetite but is less stable and larger, so viscous forces have a greater effect on the particle, which decreases the capture efficiency. The magnetic properties of the magnetite silica composites are not known. From observing their behavior around magnets it can be deduced that hydrogen reduction increases the magnetic susceptibility of the material. This explains their capture efficiencies relative to the each other. Although, the capture efficiency of the dispersed magnetite is rather low it performance significantly better in the gravity fed filter for a given flowrate.

5. The recovery of magnetite by backwashing the filter was also examined. It was found that the recovery of the magnetite particles was dependent on the pH. Raising the pH to around 10.8 minimizes the surface potential between the particle and the wire and therefore maximizes

the backwash capabilities (Svoboda, 1985). Additionally, demagnetizing the filter aids in the removal of particles. It was also found that a velocity of 1 cm/s is not substantial enough to dislodge the particles, but at 6.7 cm/s the particles are removed quicker and easier from the Frantz filter. It was also found that the dispersed particles could be recovered with distilled water alone at a velocity of 1 cm/s from the Frantz filter. These particles are easier to recover because they already contain favorable surface interactions between the wires, which are unfavorable to their capture. It should be noted that in some cases more than 100% recovery was observed but this is due to errors in approximation and fouling of the filter. Examining particle recovery from the gravity fed filter is more accurate because new stainless steel wool was used for each filtration. The filter was demagnetized and flushed at a rate of 22.1 cm/s with water of pH 10.9. The total amount of particles recovered during this backwash was 88.8%.

Design recommendations

The gravity fed filter provided the highest capture efficiencies and is recommended for industrial use. The gravity fed filter used in this bench scale experiment was 14 cm long. It had a packing fraction of stainless steel wool of 0.68 grams/ml and induced magnetism of 0.5 Tesla in the column. These parameters will provide a capture efficiency of >99% for magnetite. I believe that increasing the columns length to 0.5 meters and magnetic flux to 2 Tesla would be advantageous as to capture most all of the particles. One industrial HGMS that induced this flux required 400 kW of power to operate and this power will be assumed (Mular 2002). To backwash the column use water with a pH of 10.5 to 11 and demagnetize the column. The column can be demagnetized by oscillating the magnetic flux through the column and decreasing the magnitude of oscillations. A backwash velocity of 22 cm/s is more than enough. Further research should be completed but a backwash of 6 cm/s is more practical and will be assumed to be acceptable for this design. The cost of power consumption was calculated from the average power cost in the Midwest and the cost of the stainless steel was calculated from the price of stainless steel wool on Grainger International Inc website. The dimensional parameters and backwash conditions and an itemized cost estimate are summarized in the following tables. A basic schematic is also shown below.

Table 16. Design dimensions and backwash parameters.

Parameter	Value	Units
Column Length	0.5	m
Column Diameter	1	m
Slurry Flowrate	113 (1790)	L/s (gpm)
Packing Fraction	0.68	g/ml
Induced Magnetism	2	T
Power Required	400	kW
Backwash Flowrate	188 (2980)	L/s (gpm)
Backwash pH	10.5-11	

Table 17. Itemized Cost Estimate.

Item	Cost	Units
Filter Replacement	7140	$/filter
Power Consumption	554	$/day
Power Consumption	0.0056	cents/L

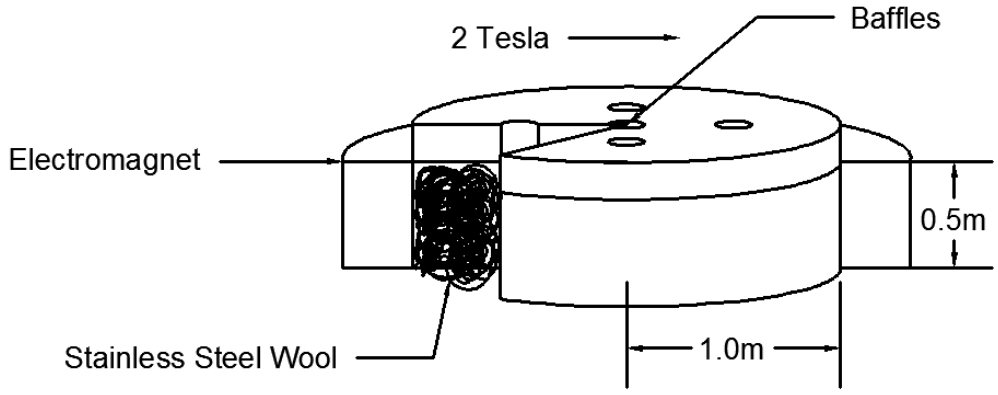

Figure 44. Basic Design Schematic of proposed HGMS.

Future research recommendations

Under the conditions presented in this research, it was found that the HGMS of nanoscale magnetite is feasible. Further work can substantiate these findings and make observations on parameters that were not changed in this research. The magnetic flux is a parameter that can be changed to increase the capture efficiencies to higher levels. The capture efficiency in the gravity fed filter was 99.8% for magnetite. It may be increased by another degree of magnitude, which is desirable, by increasing the magnetic flux. Additionally, the silica coated commercial particles and the silica magnetite particles had relatively high capture efficiencies at 96.7% and 97.9% and could potentially be captured at high enough efficiencies for industrial use with an increase in the magnetic flux imposed on the particles. The dispersed magnetite particles were the most difficult to capture. It would be useful to see how the magnetic flux affects their capture. In addition to increasing the magnetic flux, a longer column could be used which would increase the residence time in the filter at a given velocity and definitely enhance the capture of the particles. The filter could be further optimized by changing the material in the filter and the packing faction.

Larger scale experiments should be conducted on the gravity fed filter. The point at which the filter becomes saturated is not known, and determining the point at which the filter either becomes clogged or losses capture efficiency will justify the timing of backwashes. If the radius of the filter is increased the hydraulics of the filter may change. If the velocity is greater for a larger filter the capture efficiency may decrease.

A method to determine the particle size distributions of the slurry would provide valuable insight on the size of the particles being captured. While dynamic light scattering has shown that some of the supernatant contained particles about 15 nm in size, there are most likely aggregates present in the slurry. It would also be useful to obtain a size distribution for the silica and dispersed particles and compare them to the magnetite particles. This would provide further insight when comparing all of their capture efficiencies.

References

Akoto, I.Y. Mathematical modeling of high-gradient mangetic separation devices. IEEE Transactions on Magnetics, Vo. Mag-13, No. 5, 1486-1489 (1977).

Bean, C.P. Hysteresis loops of mixtures of ferromagnetic micropowders. Journal of Applied Physics, Volume 26, Number 11, 1381-1383 (1955).

Bellis, Mary (1997). "Electromagnet." About.com Inventors, <http://inventors.about.com/library/inventors/blelectromagnet.htm>, (1997).

Birss, R.R.; Gerber, R.; Parker, M.R.; Sheerer, T.J. Theory and Performance of axial magnetic filters in laminar flow conditions. IEEE Transactions on Magnetics, Vol. Mag-14, No. 5, 389-391 (1978).

Bleaney, B.I. Electricity and Magnetism. Oxford University Press, Volume 1, 98-125 (1989).

Chang, Shu-Chi; Anderson, Tracey I.; Bahrman, Sarah E.; Gruden, Cyndee L.; Khijniak, Anna I.; Adriaens, Peter. Comparing recovering efficiency of immunomagnetic separation and centrifugation of mycobacteria in metalworking fluids. J Ind Microbiol Biotechnol, Vol 32, 629-638 (2005).

Chin, Ching-Ju Monica; Chen, Pei-Wen; Wang, Li-Jen. Removal of nanoparticles from CMP wastewater by magnetic seeding aggregation. Chemosphere, Vol 63, 1809-1813 (2006).

Clarkson, C.J.; Kelland, D. Model for calculation of capture radii of a high gradient magnetic separator at moderate Reynolds numbers. IEEE Transactions on Magnetics, Vol. Mag-12, No. 6, 901-903 (1976).

Cotton, Gregory B.; Eldredge Bradley H. Nanolevel Magnetic Separation Model Considering Flow Limitations. Separation Science and Technology, Vol. 37, No. 16, pp. 3755-3779 (2002).

Ditsch, Andre; Lindenmann, Simon; Laibinis, Paul E.; Wang, Daniel I. C.; Hatton, T. Alan. High-gradient magnetic separation of magnetic nanoclusters. Ind. Eng. Chem. Res. 44, 6824-6836 (2005).

Ebner, A.D.; Ritter, J.A.; Ploehn, H.J. Feasibility and limitations of nanolevel high gradient magnetic separation. Separation and Purification Technology 11, 199-210 (1997).

Ebner, Armin D.; Ritter, James A. New Correlation for the capture cross section in high-gradient magnetic separation. AIChE Journal, Vol. 47, No. 2, 303-313 (2001).

Frantz, S.G. "Magnetic Separation Method and Means." U.S. Patent office 2,056,426 May 31, 1932.

Frantz, S.G. "Magnetic Separator." U.S. Patent office 2,074,085 May 20, 1935.

Friedlaender[1], F.J.; Gerber, R.; Kurz, W.; Birss, R.R. Particle Motion near and capture on single spheres in HGMS. IEEE Transactions on Magnetics, Vol. Mag-17, No. 6, 2801-2803 (1981)

Friedlaender[2], F.J.; Gerber, R.; Henkel, H-P; Briss R.R. Particle buildup on single spheres in HGMS. IEEE Transasctions on Magnetics, Vol. Mag-17, No. 6, 2804-2806 (1981)

Gerber[1], Richard; Birss, Robert R. High Gradient Magnetic Separation. *Research Studies Press*. A division of John Wiley & Sons LTD (1983).

Gerber[2], Richard; Takayasu M.; Friedlaender F. J.. Generalization of HGMS Theory: The Capture of Ultra-Fine Particles. IEEE Transactions on Magnetics, Vol. Mag-19, No. 5 (1983).

Gerber, Richard. Magnetic filtration of ultra-fine particle. *IEEE Transactions on Magnetics*, Vol. MAG-20, No. 5 (1984).

Gerber, R; Krist, P; Tarrant, L. The retention of strongly magnetic particles in single wire HGMS. IEEE Transactions on Magnetics, Vol. 32, No. 5, 5100-5102 (1996).

Greenberg, Arnold E.; Clesceri, Lenore S.; Eaton, Andrew D. Standard Methods for the Examination of Water and Wastewater. American Public Health Association, American Water Works Association, Water Environment Federation, Edition 18, 3.65-3.68

Gunther, C. Godfrey. Electro-magnetic ore separation. Hill Publishing Companing, New York USA. Digitalized by Google Books (1909).

Hayashi, K.; Uchiyama, S. On particle trajectory and capture efficiency around many wires. IEEE Transactions on Magnetics, Vol. MAG-16, No. 5 (1980).

Hollingworth, M.; Neset, J.E.; Finch, J.A. The buildup model of HGMS modified for field-dependent susceptibility minerals. Canadian Institute of Mining and Metallurgy, Vol. 23, No. 4, 479-480 (1984).

Hubbuch, Jurgen J.; Matthiesen, Dennis B.; Hobley, Timothy J.; Thomas, Owen R.T. High gradient magnetic separation versus expanded bed adsorption: a first principle comparison. Bioseparation, Vol 10, No 1-3, 99-112 (2001).

Iannicelli, Joseph; Millman, Nathan; Stone, William J. D. "Process for improving the brightness of clays." U.S. Patent Office 3,471,011 October 7, 1969.

Kolm, Henry H. "Magnetic Device." United States Patent Office 3,567,026 March 2, 1971.

Leitermann, W.; Friedlaender, F.J.; Gerber, R.; Hwang, J.Y.; Emory, B.B. Collection of micron-sized particles at high velocities in HGMS. IEEE Transactions on Magnetics, Vol. Mag-20, No. 5, 1174-1176 (1984).

Liu, Jing-Fu; Zhao, Zong-Shan; Jiang, Gui_bin. Coating Fe3O4 Magnetic nanoparticles with humic acid for high efficient removal of heavy metals in water. Environ. Sci. Technol. 42, 6949-6954 (2008).

Luborsky, Fred E. High gradient magnetic separation: theory versus experiment. IEEE Tranasactions On Magnetics, Vol. Mag-11, No. 6, 1696-1700 (1975).

Luborsky, F.E.; Drummond, B.J. Buildup of particles on fibers in a high field-high gradient separator. IEEE Transactions on Magnetics, Vol. Mag-12, No. 5, 463-465 (1976).

Mera-Martinez, M.E. Espinosa-Pesqueira, R. Perez-Herandez, J. Arenas-Alatorre. Synthesis of magnetite (Fe_3O_4) nanoparticles without surfactants at room temperature. Materials Letters, Vol 61, 4447-4451 (2007).

Moeser, Geoffrey D.; Roach, Kaitlin A.; Green, William H.; Laibinis, Paul E.; Hatton, Alan T. Water-Based Magnetic Fluids as Extractants for Synthetic Organic Compounds. Ind. Eng. Chem. Res. 41, 4739-4749 (2002).

Moeser, Geoffrey D.; Roach, Kaitlin A.; Green, William H.; Hatton, T. Alan. High-gradient magnetic separation of coated magnetic nanoparticles. AIChE Journal Vol. 50, No. 11 (2004).

Nriagu, Jerome O.; Pacyna, Jozef M. Quantitative assessment of worldwide contamination of air, water and soils by trace metals. Nature, Vol. 333, (1988).

Oberteuffer, John A. High Gradient Magnetic Separation. IEEE Transactions on Magnetics, Vol. Mag-9, No. 3, 303-306 (1973).

Oberteuffer, John A. Magnetic Separation: a Review of Principles, Devices, and Applications. IEEE Transactions on Magnetics, Vol. Mag-10, No. 2 (1974).

Oder, R. R.; Price, C. R. Brightness Beneficiation of Kaolin Clays by Magnetic Treatment. Tappi, Vol. 56, Journal issue 10 (1973).

Oder, R. R. High Gradient Magnetic Separation Theory and Applications. IEEE Transactions on Magnetics, Vol. Mag-12, No. 5 (1976).

Pankhurst, Q.A.; Connolly, J.; Jones, S.K.; and Dobson, J. Applications of magnetic nanoparticles in biomedicine. J. Phys. D: Appl. Phys., Vol 36, R167-R181 (2003).

Rebodos, Robert; Vikesland, Peter. Effects of Oxidation on the Magnetization of Nanoparticulate magnetite. Langmuir Article, 26 (22), 16745-16753 (2010).

Schewe, H; Takaysu, Makoto; Friedlaender, Fritz J. Observation of particle trajectories in an HGMS Single-Wire System. IEEE Tansactions on Magnetics, Vol. Mag-16, No. 1, 149-154 (1980).

Scott, William Taussig. The Physics of Electricity and Magnetism. John Wiley & Sons, Inc. (1959).

Sheere, T.J.; Parker, M.R.; Friedlaender, F.J.; Birss R.R. Theory of capture of weakly magnetic particles in random matrices in the longitudinal configuration. IEEE Transactions on Magnetics, Vol. Mag-17, No. 6, 2807-2809 (1981).

Shen, Lifen; Laibinis, Paul E.; Hatton, Alan T. Aqueous magnetic fluids stabilized by surfactant bilayers. Journal of Magnetism and Magnetic Materials, Vol 1994, 37-44 (1999).

Stolarski, Mathias; Eichholz, Christian; Fuchs, Benjamin; Nirschl, Hermann. Sedimentation acceleration of remanent iron oxide by magnetic flocculation. China Particuology, Vol 5, 145-150 (2007).

Svoboda, Jan; Corrans, Ian J. The removal of particles from the matrix of a high gradient magnetic separator. IEEE Transactions on Magnetics, Vol. Mag-21, No. 1, 53-57, January 1985.

Svoboda, J; Fujita, T. Recent developments in magnetic methods of material separation. Minerals Engineering, Vol 16, 785-792 (2003).

Takayasu[1], Makoto; Gerber, Richard; Friedlaender, F.J. The collection of strongly magnetic particles in HGMS. Journal of magnetism and Magnetic Materials, 40, 204-214 (1983).

Takayasu[2], M.; Gerber, R.; Friedlaender. Magnetic separation of submicron particles. IEEE Transactions on Magnetics, Vol. Mag-19, No. 5 (1983).

Takayasu, M; Hwang, Jiann-Yang; Friedlaender, Fritz J.; Petrakis, Leon; Gerber, Richard. Magnetic Separation Utilizing a Magnetic Susceptibility Gradient. IEEE Transactions on Magnetics, Vol. Mag-20, No. 1 (1984).

Tratynek, Paul G.; Johnson, Richard L. (2006). Nanotechnologies for environmental cleanup. Nanotoday, Volume 1, Number 2.

Tsukamoto, O.; Ohizumi, T. Feasibility study on separation of several tens nanometer scale particles by magnetic field-flow-fractionation technique using superconducting magnet. IEEE Transactions on applied superconductivity, Vol. 5, No. 2 (1995).

Uchiyama, S.; Kondo, S.; Takaysu, M. Performance of parallel stream type magnetic filter for hgms. IEEE Transactions on Magnetics, Vol. Mag-12, No. 6, 895-897 (1976).

Uchiyama, S.; Kurinobu, S.; Kumazawa, M.; Takayasu, M. Magnetic particle buildup process in parallel stream type HGMS filter. IEEE Transactions on Magnetics, Vol. Mag-13, No. 5, 1490-1492 (1977).

Wasmuth, H.-D.; Unkelbach, K.-H. Recent Developments in magnetic separation of feebly magnetic minerals. Minerals Engineering, Vol. 4, Nos 7-11, pp. 825-837 (1991).

Watson, J. H. P. Magnetic Filtration. Corning Glass Works, Corning, Newyork, 14830 (1973).

Wooding, Anthony; Kilner, Melvyn; Lambrick, David B. "Stripped" magnetic particles. Applications of the double surfactant layer principle in the preparation of water-based magnetic fluids. Journal of Colloid and Interface Science, Vol 149, No 1, 98-104 (1992).

Worm, Horst-Ulirch. On the superparamagnetic-stable single domain transition for magnetite, and frequency dependence of susceptibility. Geophys. J. Int., Vol 133, 201-206 (1998).

Yantasee, Wassana; Warner, Cynthia L.; Sangvanich, Thanapon; Addleman, Shane R.; Carter, Timothy G.; Wiacek, Robert J.; Fryxell, Glen E.; Timchalk, Charles; Warner, Marvin, G. Removal of heavy metals from aqueous systems with thiol functionalized superparamagnetic nanoparticles. Environ. Sci. Technol., 41, 5114-5119.

Yavuz[1], C.T.; Mayo, J.T., Yean, S.; Cong, L.; Yu, W.; Falkner, J.; Kan, A; Tomson, M.; Colvin, V.L. Particle size dependence of nano-magnetite in arsenic removal. Advanced Processing of Metals and Materials, Volume 3 – Thermo and Physicochemical Principles: Special Materials and Aqueous and Electrochemical Processing, 221-228 (2006).

Yavuz[2], Cafer T; Mayo, J.T.; Yu, William W.; Prakash, Arjun; Falkner, Josha C.; Yean, Sujin; Cong, Lili; Shipley, Heather J.; Kan, Amy; Tomson, Mason; Natelson, Douglas; Colvin, Vicki L. Low-field magnetic separation of monodisperse Fe_3O_4 nanocrystals. Science, Vol 314, 964-967 (2006).

Yuan, Peng; Liue, Dong; Fan, Mingde; Yang, Dan; Zhu, Runliang; Ge, Fei; Zhu, JianXi; He, Hongping. Removal of hexavalent chromium [Cr(VI)] from aqueous solution by the diatomite-supported/unsupported magnetite nanoparticles. Journal of Hazardous Materials, Vol 173, 614-621 (2010).

Zhang, Yang; Chen, Yongsheng; Westerhoff, Paul; Hristovski, Kiril; Crittenden, John C. Stability of commercial metal oxide nanoparticles in water. Water Research, Vol. 42, 2204-2212 (2008).

Appendix 1 – List of Variables

B – Magnetic induction

H – Field Strength

μ_m – Magnetic permeability of a material

μ_o – Magnetic permeability of free space

ŭ – Magnetic dipole

M – Magnetization

M_p – Magnetization of a particle

M_{sp} – Saturation magnetization of a particle

χ – Difference in the magnetic susceptibility of to materials

χ_m – Magnetic susceptibility of a material

q – Electric charge of a particle

***v* – Instantaneous velocity of a particle**

τ – Torque

A – Area

I – Current

U – Potential energy

V – Volume

V_p – Volume of a particle

k – Boltzmann's constant

T – Temperature

F_m – Magnetic force

F_v – Viscous force

F_g – Gravity force

F_d – Diffusion force

a – Radius of a wire

b – Radius of a particle

R – Radius of a particle

r – Distance vector

r_a – Distance vector relative to the radius of a wire (r/a)

η – Viscosity

g – Gravity

ρ – Density

c – Particle number concentration

D – Diffusion coefficient

ε – Permeability of a liquid

ψ_o – Double layer potential

K_s – Magnetic velocity

N – Number of particles

F – Filling factor

G – Geometry factor

L – Length of filter

K_{mv} – Fluid drag limit

K_{md} – Fluid diffusion limit

B – Buildup of particles

C – Fraction of particles captured